AMERICAN SOCIETY FOR MICROBIOLOGY | Journal of Bacteriology®

RESEARCH ARTICLE

Association of *Mycobacterium* Proteins with Lipid Droplets

Richard M. Armstrong,[a] Dominique C. Carter,[a]* Samantha N. Atkinson,[a] Scott S. Terhune,[a] Thomas C. Zahrt[a]

[a]Department of Microbiology and Immunology, Center for Infectious Disease Research, Medical College of Wisconsin, Milwaukee, Wisconsin, USA

ABSTRACT *Mycobacterium tuberculosis* is a global pathogen of significant medical importance. A key aspect of its life cycle is the ability to enter into an altered physiological state of nonreplicating persistence during latency and resist elimination by the host immune system. One mechanism by which *M. tuberculosis* facilitates its survival during latency is by producing and metabolizing intracytoplasmic lipid droplets (LDs). LDs are quasi-organelles consisting of a neutral lipid core such as triacylglycerol surrounded by a phospholipid monolayer and proteins. We previously reported that PspA (phage shock protein A) associates with LDs produced in *Mycobacterium*. In particular, the loss or overproduction of PspA alters LD homeostasis in *Mycobacterium smegmatis* and attenuates the survival of *M. tuberculosis* during nonreplicating persistence. Here, *M. tuberculosis* PspA ($PspA_{Mtb}$) and a Δ*pspA M. smegmatis* mutant were used as model systems to investigate the mechanism by which PspA associates with LDs and determine if other *Mycobacterium* proteins associate with LDs using a mechanism similar to that for PspA. Through this work, we established that the amphipathic helix present in the first α-helical domain (H1) of PspA is both necessary and sufficient for the targeting of this protein to LDs. Furthermore, we identified other *Mycobacterium* proteins that also possess amphipathic helices similar to PspA H1, including a subset that localize to LDs. Altogether, our results indicate that amphipathic helices may be an important mechanism by which proteins target LDs in prokaryotes.

IMPORTANCE *Mycobacterium* spp. are one of the few prokaryotes known to produce lipid droplets (LDs), and their production has been linked to aspects of persistent infection by *M. tuberculosis*. Unfortunately, little is known about LD production in these organisms, including how LDs are formed, their function, or the identity of proteins that associate with them. In this study, an established *M. tuberculosis* LD protein and a surrogate *Mycobacterium* host were used as model systems to study the interactions between proteins and LDs in bacteria. Through these studies, we identified a commonly occurring protein motif that is able to facilitate the association of proteins to LDs in prokaryotes.

KEYWORDS *Mycobacterium*, *Mycobacterium tuberculosis*, phage shock protein, PspA, amphipathic helix, latency, lipid droplets, nonreplicating persistence

Mycobacterium tuberculosis is an acid-fast bacillus and is responsible for the respiratory disease tuberculosis (TB). In 2016, this bacterium was responsible for ~10.4 million cases of TB and more than 1.7 million deaths (1), making *M. tuberculosis* a leading cause of death in the world due to an infectious agent. The World Health Organization currently estimates that 1.7 billion people are latently infected with *M. tuberculosis* (1). During latency, *M. tuberculosis* resides within granulomatous lesions in a metabolically altered state of nonreplicating persistence. The ability of *M. tuberculosis* to establish, maintain, and reactivate from nonreplicating persistence is a critical aspect of its life cycle, contributing to the continued circulation of this pathogen within the human population.

Received 23 April 2018 **Accepted** 7 May 2018

Accepted manuscript posted online 14 May 2018

Citation Armstrong RM, Carter DC, Atkinson SN, Terhune SS, Zahrt TC. 2018. Association of *Mycobacterium* proteins with lipid droplets. J Bacteriol 200:e00240-18. https://doi.org/10.1128/JB.00240-18.

Editor Thomas J. Silhavy, Princeton University

Address correspondence to Thomas C. Zahrt, tzahrt@mcw.edu.

* Present address: Dominique C. Carter, Office of International Science & Engineering, Office of the Director, National Science Foundation, Alexandria, Virginia, USA.

One strategy thought to be utilized by *M. tuberculosis* to persist during latency is the production of lipid droplets (LDs) which can be used as an energy reservoir under conditions of stress. LDs are quasi-organelles comprised of a neutral lipid core such as triacylglycerol and are surrounded by a phospholipid monolayer and proteins. Several lines of evidence indicate that LDs regulate key aspects of the *M. tuberculosis* life cycle. Bacilli present in sputum samples derived from TB patients with active disease possess intracytoplasmic LDs (2). In addition, environmental conditions and/or cell types thought to be encountered by *M. tuberculosis* within the granuloma are capable of inducing the production of LDs within *M. tuberculosis* and other disease-causing mycobacterial species (3–7). Finally, *M. tuberculosis* mutants that are defective in their ability to synthesize or hydrolyze triacylglycerol exhibit survival and/or reactivation defects *in vitro* and *in vivo* (4–11). These results suggest that proteins involved in LD production, maintenance, and/or mobilization may be rational targets for therapeutic intervention.

While LDs are produced by nearly all eukaryotes, only a limited number of prokaryotes, including species of *Mycobacterium* and *Rhodococcus*, have been shown to produce LDs (reviewed in references 12–14). Consequently, much less is known about LDs in bacteria, including their proteomic composition or the features that target proteins to these structures. To date, several hundred proteins have been identified in the LD proteome of *Rhodococcus* (15, 16). In contrast, only seven proteins thus far have been described in the proteome of LDs from *Mycobacterium* (17, 18). Five of these proteins are predicted to function in the synthesis and/or hydrolysis of TAG, including Tgs1 (BCG_3153c), Tgs2 (BCG_3794c), BCG_1169c, BCG_1489c, and BCG_1721 (18). Of the other two determinants, Acr (HspX) is a stress-responsive protein that functions as an ATP-independent chaperone (9, 11, 18) and PspA is a member of the phage shock protein A (PspA) family (17). While PspA has been observed on LDs produced in *Rhodococcus*, its function in these organisms remains unknown (63, 64). In *Mycobacterium smegmatis*, the loss or overproduction of PspA alters the size distribution of LDs produced by these organisms (17). In *M. tuberculosis*, the loss or overproduction of PspA attenuates survival during nonreplicating persistence (17). These observations indicate that PspA may play an important role in the physiology and/or persistence of *M. tuberculosis* within the host during latency.

PspA is a member of an evolutionarily conserved family of proteins (PspA/Vipp1/IM30) that are found in bacteria, algae, and plants (reviewed in reference 19). In most Gram-positive and Gram-negative bacteria, PspA binds to the inner face of the plasma membrane and regulates plasma membrane homeostasis under conditions of cell envelope stress (19–21). In plants, algae, and photosynthetic bacteria, the PspA ortholog, Vipp1 (vesicle-inducing protein in plastids 1), binds to the inner membrane of chloroplasts where it regulates the biogenesis and maintenance of these organelles (22–25). While members of the PspA/Vipp1/IM30 protein family are generally unrelated at the amino acid level, they all possess a largely α-helical secondary structure and are able to form large homo-oligomeric complexes that assume ring- and/or rodlike superstructures (17, 26–30). Furthermore, these proteins share the ability to bind phospholipids and membranes through an amphipathic helix that resides within the N and/or C terminus of these proteins (23, 24, 31).

In this study, PspA from *M. tuberculosis* ($PspA_{Mtb}$) and a Δ*pspA M. smegmatis* mutant were used to delineate the proteomic composition of *Mycobacterium* LDs and begin interrogating the mechanism by which proteins are able to target LDs in prokaryotes. Through these studies, we have determined that the amphipathic helix present within the H1 domain of $PspA_{Mtb}$ is both necessary and sufficient for this protein to bind *Mycobacterium* LDs. Furthermore, amphipathic helices with similarity to the $PspA_{Mtb}$ H1 domain are present in other *M. smegmatis* proteins, including a subset that localize to *Mycobacterium* LDs. In summary, our data implicate amphipathic helices as an important mechanism by which proteins associate with LDs in prokaryotes.

RESULTS

H1 domain is necessary and sufficient for localization of $PspA_{Mtb}$ to LDs. $PspA_{Mtb}$ is largely α-helical and contains five distinct α-helical domains (Fig. 1A) (17). As amphipathic helices are one motif used by eukaryotic proteins to target LDs (32–36), $PspA_{Mtb}$ was first analyzed using Heliquest to identify possible amphipathic helices (37). Results from this search indicated the presence of an amphipathic helix in the N-terminal H1 domain of $PspA_{Mtb}$. The 18 residues comprising this motif have a hydrophobic moment (μH) of 0.543 and a mean hydrophobicity (H) of 0.589 (Fig. 1B). This domain is highly conserved in PspA family members (31), including in *Mycobacterium* species (Fig. 1C). To investigate the importance of this domain for $PspA_{Mtb}$ localization to LDs, a variant of $PspA_{Mtb}$ lacking the first 22 amino acids which includes the H1 domain ($PspA_{Mtb}\Delta H1$) was generated (Fig. 1A). This derivative, along with wild-type $PspA_{Mtb}$, was produced in an *M. smegmatis* Δ*pspA* strain under conditions promoting LD production. The protein was then localized by Western blotting following subcellular fractionation. Wild-type $PspA_{Mtb}$ localized predominantly to LDs (Fig. 1D), similar to that previously reported (17). The higher molecular weight banding pattern observed is due to the presence of SDS-resistant $PspA_{Mtb}$ multimers, a characteristic that has been observed previously (17). In contrast, $PspA_{Mtb}\Delta H1$ was observed exclusively in the cytoplasmic compartment, indicating that the H1 domain is necessary for $PspA_{Mtb}$ to localize to LDs (Fig. 1E). MprB and GroES, membrane and cytoplasmic control proteins, respectively, were present in their expected subcellular compartments, confirming the fractionation procedure (Fig. 1D and E). Thus, the H1 domain is necessary for $PspA_{Mtb}$ to associate with LDs.

To investigate if the removal of the N-terminal 22 amino acids of $PspA_{Mtb}$ alters global protein structure, $PspA_{Mtb}$ and $PspA_{Mtb}\Delta H1$ were produced and purified in *Escherichia coli* (see Fig. S1 in the supplemental material). The oligomeric nature of the purified proteins was then characterized by analyzing their mobility on a 10 to 50% continuous sucrose gradient alongside protein standards of known mass and by negative-stain electron microscopy (EM). Following ultracentrifugation, wild-type $PspA_{Mtb}$ localized predominantly to fraction 18, between thyroglobulin (fraction 14; ~670 kDa) and blue dextran (fraction 23). In addition, $PspA_{Mtb}$ formed spheroid and rodlike superstructures (Fig. 1F and G), similar to that seen previously (17). In contrast, $PspA_{Mtb}\Delta H1$ localized primarily to fraction 23, similar to blue dextran (>2,000 kDa) (Fig. 1F). When analyzed by negative stain EM, $PspA_{Mtb}\Delta H1$ also formed spheroids and rodlike superstructures (Fig. 1G). While these results indicate that the removal of the H1 domain does not induce gross structural changes to $PspA_{Mtb}$, the loss of this region does shift the fractionation pattern within the sucrose gradient to the right, possibly reflecting an increased propensity of the $PspA_{Mtb}\Delta H1$ variant to form larger rodlike superstructures, as indicated by negative-stain EM (Fig. 1F and G).

Finally, to determine if the H1 domain is also sufficient to facilitate the localization of $PspA_{Mtb}$ to LDs, the first 22 amino acids of $PspA_{Mtb}$ were fused in single copy, or in multiple tandem copies, to the N terminus of green fluorescent protein mutant GFPmut3 (Fig. 1H). The ability of these H1-GFPmut3 chimeras to localize to *M. smegmatis* LDs was then assessed. While GFPmut3 alone partitioned completely in the cytoplasmic compartment (Fig. 1I), the addition of either one or three copies of the $PspA_{Mtb}$ H1 domain to GFPmut3 altered the localization such that a predominant fraction of GFP now localized to LDs (Fig. 1I). Altogether, these results indicate that the H1 domain of $PspA_{Mtb}$ is both necessary and sufficient for $PspA_{Mtb}$ to localize to LDs.

PspA from *Rhodococcus* contains an amphipathic helix in its H1 domain and localizes to LDs when produced in *M. smegmatis*. PspA has been identified in the LD proteome of *Rhodococcus jostii* strain RHA1 ($PspA_{Rho}$) (16). $PspA_{Rho}$ is 77% identical to $PspA_{Mtb}$ at the primary amino acid level (17); however, other aspects of $PspA_{Rho}$, including the mechanism by which it localizes to LDs, remain unknown. To determine if $PspA_{Rho}$ is α-helical and possesses an amphipathic helix similar to that of $PspA_{Mtb}$, $PspA_{Rho}$ was analyzed using Psipred and Heliquest (37). $PspA_{Rho}$ forms five α-helical domains (Fig. 2A), similar to $PspA_{Mtb}$. Furthermore, the H1 domain of $PspA_{Rho}$ (residues

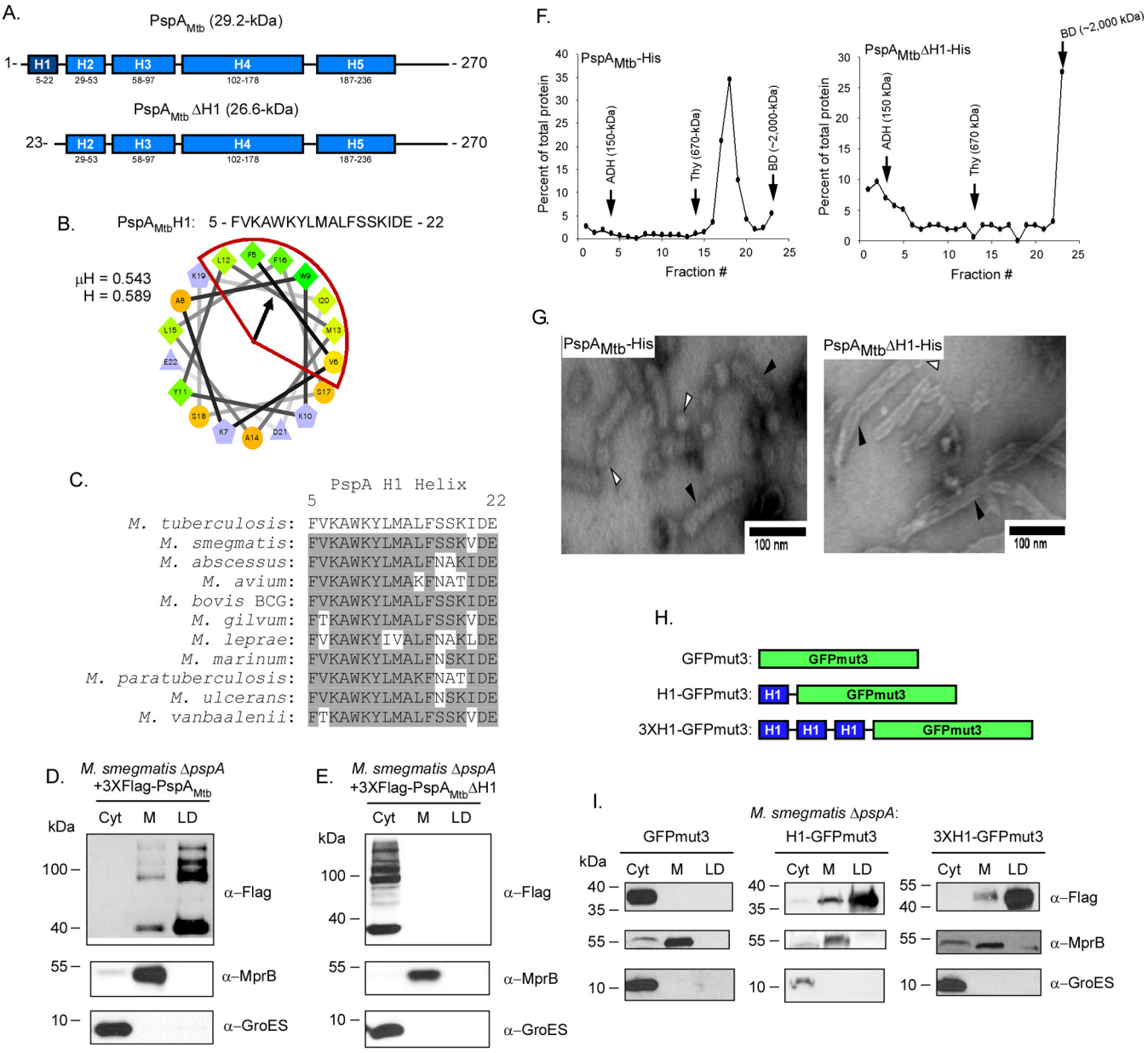

FIG 1 Helix 1 is necessary and sufficient for PspA localization to lipid droplets. (A) Schematic of Psipred-predicted helices (blue segments; helix 1 in dark blue) of full-length PspA$_{Mtb}$ (top) and helix-1-truncated PspA$_{Mtb}$ (PspA$_{Mtb}$ΔH1) (bottom). (B) Helical wheel diagram of helix 1 comprising residues 5 to 22 of the protein. The hydrophobic face of the amphipathic helix is highlighted in red. Hydrophobicity (H) and mean hydrophobic moment (μH) values are noted. The arrow indicates the angle of the mean hydrophobic moment. (C) The PspA H1 helix (residues 5 to 22) from various mycobacterial species was aligned using Clustal W (DNASTAR; Lasergene, Madison, WI). Amino acid residues that are identical are shaded gray. PspA from the following species were used: *Mycobacterium tuberculosis*, *Mycobacterium smegmatis*, *Mycobacterium abscessus*, *Mycobacterium avium*, *Mycobacterium bovis* BCG, *Mycobacterium gilvum*, *Mycobacterium leprae*, *Mycobacterium marinum*, *Mycobacterium paratuberculosis*, *Mycobacterium ulcerans*, and *Mycobacterium vanbaalenii*. (D and E) Western blots showing localization of 3×Flag-PspA$_{Mtb}$ (D) and 3×Flag-PspA$_{Mtb}$ΔH1 (E) following production in *M. smegmatis* Δ*pspA*. PspA derivatives were detected using anti-Flag antibody. Anti-GroES and anti-MprB antibodies were used to detect control proteins. Fraction abbreviations: Cyt, cytosol; M, membrane; LD, lipid droplets. The images shown are representative of experiments performed in triplicate. (F) Distribution of PspA$_{Mtb}$-His (left) and PspA$_{Mtb}$ΔH1-His (right) following ultracentrifugation on 10 to 50% continuous sucrose gradients. Fractions were collected from top to bottom of the gradient tubes and are displayed on the *x* axis. Protein concentration as a percentage of total protein detected for each sample is displayed on the *y* axis. Arrows indicate the fractions in which molecular weight standards localized in gradients that were run in parallel: ADH, alcohol dehydrogenase (150 kDa); Thy, thyroglobulin (670 kDa); BD, blue dextran (~2,000 kDa). (G) Negative-stain electron microscopy of PspA$_{Mtb}$-His (left) or PspA$_{Mtb}$ΔH1-His (right). Protein was purified from fraction 18 (PspA$_{Mtb}$-His) or 23 (PspA$_{Mtb}$ΔH1-His), stained with uranyl acetate, and examined at ×100,000 magnification. White arrowheads indicate spheroid structures, and black arrowheads indicate rodlike superstructures. (H) Schematic of 3×Flag-GFPmut3 constructs with either 1, 3, or no H1 tag(s) cloned at the N terminus. (I) Western blot showing localization of wild-type and mutant GFPmut3 variants following production in *M. smegmatis* Δ*pspA*. GFPmut3 variants were detected using anti-Flag antibody. Anti-GroES and anti-MprB antibodies were used to detect control proteins. Fraction abbreviations: Cyt, cytosol; M, membrane; LD, lipid droplets. The images shown are representative of experiments performed in triplicate.

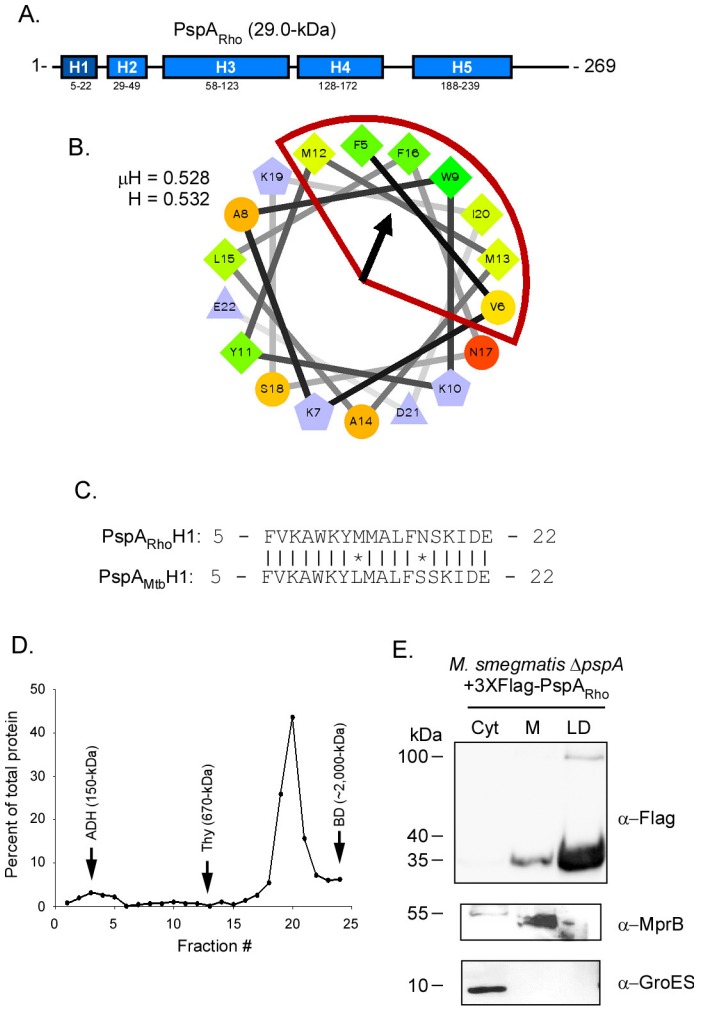

FIG 2 PspA from *Rhodococcus* localizes to *Mycobacterium* lipid droplets. (A) Schematic of Psipred-predicted helices of PspA$_{Rho}$ (blue segments; helix 1 in dark blue). (B) Helical wheel diagram of helix 1 from PspA$_{Rho}$ comprising residues 5 to 22 of the protein. The hydrophobic face of the amphipathic helix is highlighted in red. Hydrophobicity (H) and mean hydrophobic moment (μH) values are noted. The arrow indicates the angle of the mean hydrophobic moment. (C) Sequence alignment between the H1 domains of PspA$_{Rho}$ and PspA$_{Mtb}$. Vertical lines, identical residues; *, mismatched residues. (D) Distribution of PspA$_{Rho}$-His following ultracentrifugation on 10 to 50% continuous sucrose gradients. Fractions were collected from top to bottom of the gradient tubes and are displayed on the *x* axis. Protein concentration as a percentage of total protein detected for each sample is displayed on the *y* axis. Arrows indicate the fractions in which molecular weight standards localized in gradients that were run in parallel: ADH, alcohol dehydrogenase (150 kDa); Thy, thyroglobulin (670 kDa); BD, blue dextran (~2,000 kDa). (E) Western blot showing localization of 3×Flag-PspA$_{Rho}$ following production in *M. smegmatis* Δ*pspA*. PspA$_{Rho}$ was detected using anti-Flag antibody. Anti-GroES and anti-MprB antibodies were used to detect control proteins. Fraction abbreviations: Cyt, cytosol; M, membrane; LD, lipid droplets. The images shown are representative of experiments performed in triplicate.

5 to 22) is predicted to be amphipathic, with μH and H values of 0.528 and 0.532, respectively (Fig. 2B). Interestingly, the H1 domain of PspA$_{Rho}$ differs from PspA$_{Mtb}$ H1 by only two residues (L12M and S17N) (Fig. 2C). To determine if PspA$_{Rho}$ forms higher order homo-oligomers like PspA$_{Mtb}$, PspA$_{Rho}$ was produced in *E. coli*, purified, and analyzed using sucrose gradient ultracentrifugation (Fig. S1). PspA$_{Rho}$ localized predominantly to fraction 20 between the control proteins thyroglobulin (fraction 13) and blue dextran (fraction 24) (Fig. 2D). These results are similar to those observed for PspA$_{Mtb}$ (Fig. 1E). Finally, to determine if PspA$_{Rho}$ binds *Mycobacterium* LDs, the protein was produced in *M. smegmatis* Δ*pspA* under LD-inducing conditions, and its subcellular localization was assessed as described previously. PspA$_{Rho}$ was observed predomi-

nantly in the LD fraction (Fig. 2E). Importantly, control proteins, including MprB and GroES, localized to their expected compartments (Fig. 2E), confirming the fractionation procedure. Thus, $PspA_{Rho}$ is largely α-helical, possesses an amphipathic helix in its H1 domain that is nearly identical to that in $PspA_{Mtb}$, and is able to bind LDs when produced in *M. smegmatis* Δ*pspA*.

PspA from *E. coli* associates with LDs when produced in *M. smegmatis*. The ability of $PspA_{Mtb}$ and $PspA_{Rho}$ to bind LDs in *Mycobacterium* may be due to the amphipathic nature of their H1 domains. Alternatively, the ability of these proteins to associate with LDs may be due to the highly conserved residues comprising this domain. To differentiate between these possibilities, PspA from *E. coli* ($PspA_{Eco}$) was produced in *M. smegmatis* Δ*pspA* and its binding to LDs assessed. $PspA_{Eco}$ possesses a largely α-helical domain architecture (Fig. 3A) (27, 38, 39) and also contains an amphipathic helix within its H1 domain (also called AHa; residues 2 to 19) (Fig. 3B) (31); however, $PspA_{Eco}$ exhibits little to no amino acid sequence identify with $PspA_{Mtb}$ and $PspA_{Rho}$ in the H1 region (Fig. 3C) (17). We first confirmed by sucrose gradient ultracentrifugation that $PspA_{Eco}$ produced in *E. coli* homo-oligomerizes as has been reported previously (27, 28). As expected, $PspA_{Eco}$ localized predominantly to fraction 20, between thyroglobulin (fraction 13) and blue dextran (fraction 24) (Fig. 3D; Fig. S1), confirming that this protein forms higher order homo-oligomeric complexes. Interestingly, when $PspA_{Eco}$ was produced in *M. smegmatis* Δ*pspA*, the protein localized almost exclusively within the LD compartment (Fig. 3E). In contrast, the control proteins MprB and GroES were localized within the membrane and cytoplasmic compartments, respectively, as expected (Fig. 3E). Altogether, these results indicate that the ability of PspA to associate with LDs is likely due to the amphipathic nature of its H1 (AHa) domain rather than the specific amino acid residue(s) that comprises this domain.

Amino acid substitutions within the H1 domain of $PspA_{Mtb}$ reduce but do not abrogate binding to LDs. Recently, it was demonstrated that the localization of amphipathic helices to LDs is largely independent of the H or μH (35). Rather, the binding of amphipathic helices to LDs is more dependent on the number of large hydrophobic residues (I, F, L, M, W, or Y) that are present on the hydrophobic face of the helix (35). In particular, amphipathic helices with 5 or more large hydrophobic residues are able to bind LDs, with the efficiency of binding proportional to the number of large hydrophobic residues present (35). As the $PspA_{Mtb}$ H1 domain contains 6 large hydrophobic residues on its hydrophobic face (Fig. 1B), we postulated that the mutation of one or more of these residues may reduce or abrogate the ability of $PspA_{Mtb}$ to bind LDs. To test this possibility, select amino acid residues along the hydrophobic or hydrophilic face of the $PspA_{Mtb}$ H1 domain were mutated to alanine (Fig. 4A). F5, W9, and F16 were chosen for the mutations, as these residues are on the hydrophobic face of the helix and are positioned nearest the hydrophobic moment (Fig. 4A). K7 and Y11 were also chosen, as they are on the hydrophilic face of the helix and were not expected to contribute substantively to LD binding (Fig. 4A). While individual substitutions at F5 and W9 alone did not alter the distribution pattern of $PspA_{Mtb}$ relative to that of the wild-type protein (Fig. 4B and C), a substitution at F16 significantly reduced the percentage of $PspA_{Mtb}$ localized to LDs (Fig. 4B and C). Furthermore, $PspA_{Mtb}$ variants harboring two (F5A/W9A, F5A/F16A, or W9A/F16A) or three (5FA/W9A/F16A) amino acid substitutions on the hydrophobic face of the H1 helix were also reduced in their ability to bind LDs relative to that of the wild-type PspA (Fig. 4B and C). Interestingly, the level of binding of these variants was similar to that observed for the single F16A mutant even though these mutant proteins possessed 4 or fewer large hydrophobic residues on the hydrophobic face of the helix (Fig. 4B and C). $PspA_{Mtb}$ variants carrying substitutions along the hydrophilic face of the H1 domain (K7 or Y11) were also reduced in their ability to bind LDs (Fig. 4B and C), indicating that amino acid residues along the hydrophilic face of $PspA_{Mtb}$ may also contribute to LD interactions. Altogether, our results indicate that amino acids on the hydrophobic and hydrophilic faces of the H1 amphipathic helix contribute to LD binding by $PspA_{Mtb}$.

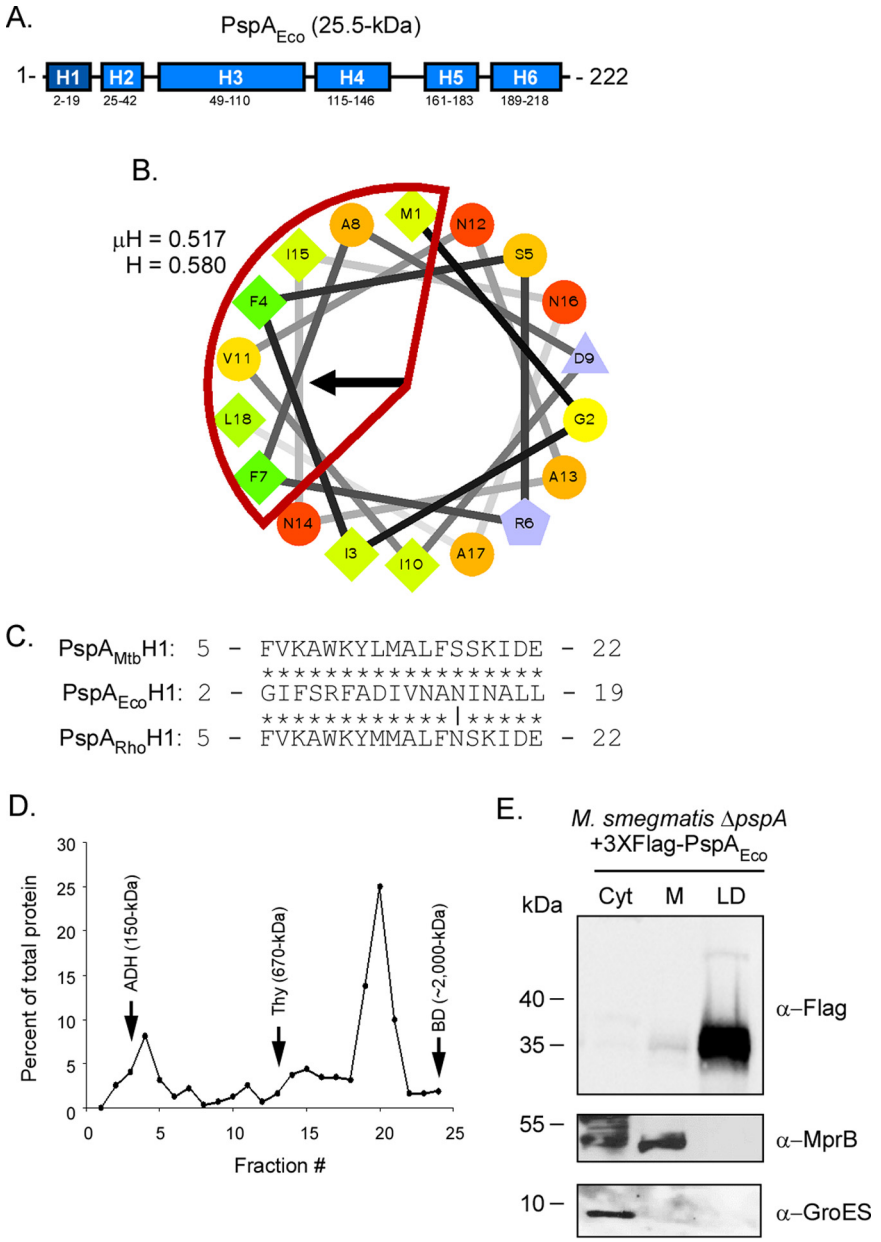

FIG 3 PspA from *E. coli* localizes to *Mycobacterium* lipid droplets. (A) Schematic of Psipred-predicted helices of PspA$_{Eco}$ (blue segments; helix 1 in dark blue). (B) Helical wheel diagram of helix 1 from PspA$_{Eco}$ comprising residues 2 to 19 of the protein. The hydrophobic face of the amphipathic helix is highlighted in red. Hydrophobicity (H) and mean hydrophobic moment (μH) values are noted. The arrow indicates the angle of the mean hydrophobic moment. (C) Sequence alignment of the H1 domain from PspA$_{Eco}$ with the H1 domains of PspA$_{Rho}$ and PspA$_{Mtb}$. Vertical line, identical residues; *, mismatched residues. (D) Distribution of PspA$_{Eco}$-His following ultracentrifugation on 10 to 50% continuous sucrose gradients. Fractions were collected from top to bottom of the gradient tubes and are displayed on the *x* axis. Protein concentration as a percentage of total protein detected for each sample is displayed on the *y* axis. Arrows indicate the fractions in which molecular weight standards localized in gradients that were run in parallel: ADH, alcohol dehydrogenase (150 kDa); Thy, thyroglobulin (670 kDa); BD, blue dextran (~2,000 kDa). (E) Western blot showing localization of 3×Flag-PspA$_{Eco}$ following production in *M. smegmatis* Δ*pspA*. PspA$_{Eco}$ was detected using anti-Flag antibody. Anti-GroES and anti-MprB antibodies were used to detect control proteins. Fraction abbreviations: Cyt, cytosol; M, membrane; LD, lipid droplets. The images shown are representative of experiments performed in triplicate.

In PspA$_{Eco}$, substitutions at single hydrophobic residues (F4E or V11E) along the hydrophobic face of the H1 (AHa) domain are sufficient to abrogate binding of this protein to lipids (31). Given our inability to completely abrogate binding of PspA$_{Mtb}$ to LDs following a substitution at one or more residues along the hydrophobic face of the

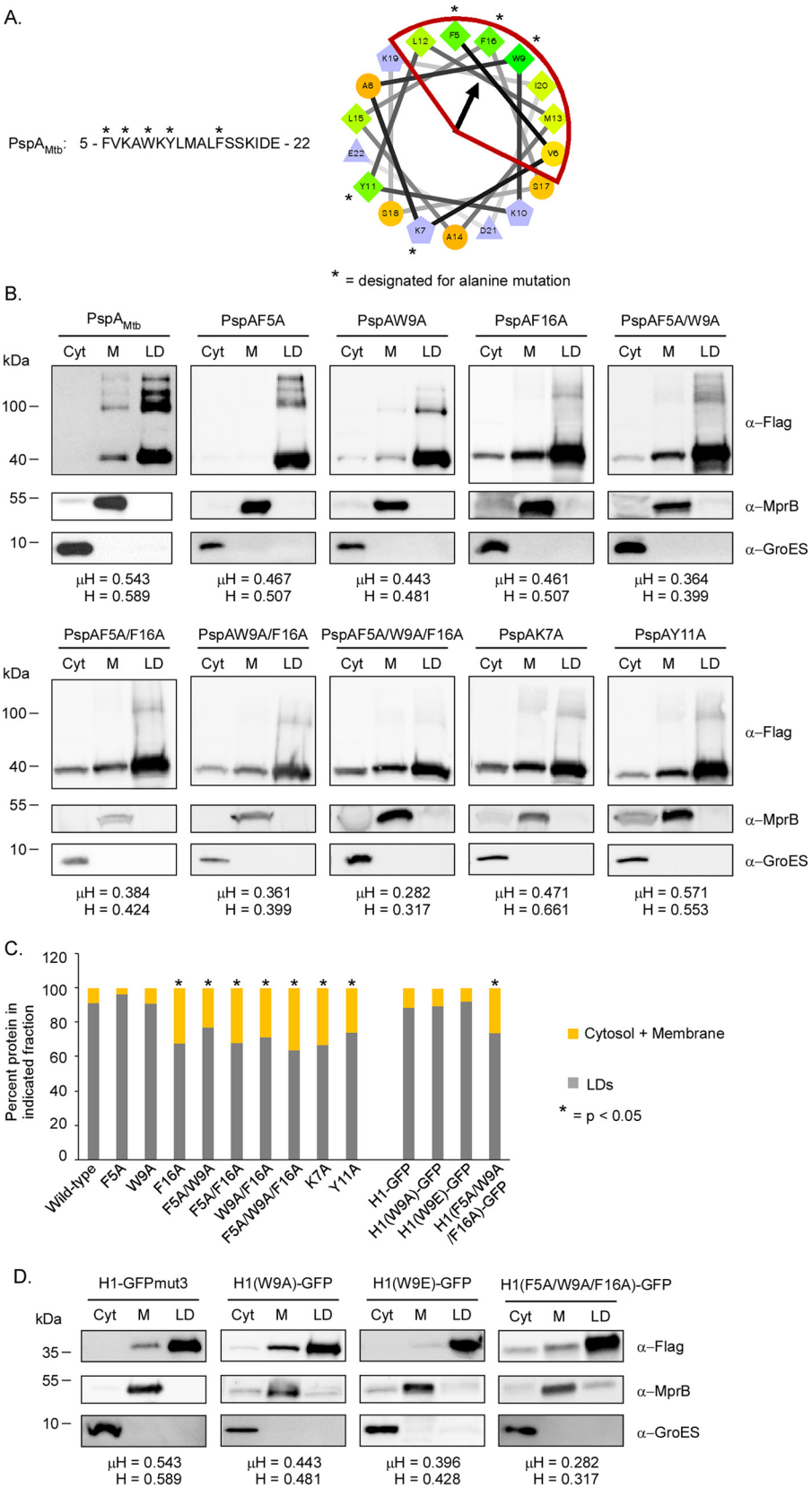

FIG 4 Impact of H1 amino acid substitutions on PspA and H1-GFP chimera localization. (A, left) Amino acid sequence of the PspA$_{Mtb}$ H1 domain (residues 5 to 22). *, residues targeted for alanine mutagenesis. (Right) Helical wheel diagram of the PspA$_{Mtb}$ H1 domain. *, mutagenized residues. The arrow indicates the angle of the mean hydrophobic moment. (B) Western blots showing localization of wild-type and mutant variants

(Continued on next page)

H1 helix, we wondered if the propensity for $PspA_{Mtb}$ to bind itself may partially mask LD-binding defects. To test this possibility, a subset of the H1 amino acid substitutions were generated in the H1-GFPmut3 chimera, including W9A, W9E, and 5FA/W9A/F16A. The resulting protein variants were then tested for their ability to associate with LDs following production in *M. smegmatis* Δ*pspA*. The localization patterns of the generated H1-GFPmut3 chimeras were similar to those observed for their full-length $PspA_{Mtb}$ counterparts (Fig. 4C and D), demonstrating that homo-oligomerization of $PspA_{Mtb}$ does not regulate H1 binding to LDs.

In summary, our results indicate that the binding of $PspA_{Mtb}$ to LDs can be achieved with as few as three large hydrophobic residues along the hydrophobic face of the H1 amphipathic helix. Furthermore, the binding of $PspA_{Mtb}$ to LDs is dependent on residues present on both the hydrophobic and hydrophilic faces of the H1 helix but is independent of homo-oligomerization of the protein.

Identification and validation of potential LD-binding amphipathic helices in other mycobacterial proteins. Six proteins have previously been identified in the LD proteome of *Mycobacterium bovis* BCG (18). To determine if any of these proteins possess amphipathic helices similar to the H1 domain of $PspA_{Mtb}$, BCG_1169c, BCG_1489c, BCG_1721, HspX (BCG_2050c), Tgs1 (BCG_3153c), and Tgs2 (BCG_3794) were analyzed using Heliquest. Of the six proteins analyzed, four contained helices which satisfied search parameter requirements, including Tgs1, BCG_1721, Tgs2, and BCG_1169c (Fig. 5). Notably, Tgs2 contained two such helices. The numbers of large hydrophobic residues present in the amphipathic helices of these proteins ranged between 4 and 5. Thus, a subset of *M. bovis* BCG proteins known to bind *Mycobacterium* LDs possess one or more amphipathic helices with similarity to the H1 domain of $PspA_{Mtb}$.

We next investigated whether $PspA_{Mtb}$ H1-like amphipathic helices exist in other proteins from *M. smegmatis*. To investigate this possibility, the complete *M. smegmatis* proteome was searched using Heliquest. The resulting candidates were then screened to identify candidates that possessed 5 or more large hydrophobic residues along the hydrophobic face of the helix (35, 37). Of the 6,602 proteins analyzed, 330 proteins (~5% of the total proteome) satisfied these search parameter criteria (see Table S2). Amphipathic helices were positioned throughout the amino acid sequences of the identified proteins, with the numbers of large hydrophobic residues ranging between 5 and 9. Importantly, MSMEG_2695, the *M. smegmatis* homolog of PspA, was present in the list.

To determine if any of the proteins identified from the Heliquest search were able to bind LDs, LDs were purified from wild-type *M. smegmatis* and treated with chloroform-methanol to extract proteins, and the resulting proteins were identified by liquid chromatography-tandem mass spectroscopy (LC-MS/MS). For these studies, LDs were isolated from three independent cultures of wild-type *M. smegmatis*. Each of these biological replicates was further split into technical triplicates prior to their injection into the mass spectrometer. Only proteins in which 3 or more peptides were observed in at least 2 of the 3 technical replicates, and in at least 2 of the 3 biological replicates,

FIG 4 Legend (Continued)
of 3×Flag-$PspA_{Mtb}$ following production in *M. smegmatis* Δ*pspA*. $PspA_{Mtb}$ was detected using anti-Flag antibody. Anti-GroES and anti-MprB antibodies were used to detect control proteins. Fraction abbreviations: Cyt, cytosol; M, membrane; LD, lipid droplets. Hydrophobicity (H) and mean hydrophobic moment (μH) values are noted for each H1 domain. The images shown are representative of experiments performed in triplicate. (C) Graph indicating the average percentages of proteins present in the lipid droplet fractions relative to the average percentages of each protein present in the cytosolic and membrane fractions. *, $P < 0.05$ versus wild-type $PspA_{Mtb}$ or H1-GFPmut3. Values were derived from experiments performed in triplicate. (D) Western blots showing localization of 3×Flag-H1-GFPmut3 and 3×Flag-H1-GFPmut3 mutant variants following production in *M. smegmatis* Δ*pspA*. H1-GFPmut3 derivatives were detected using anti-Flag antibody. Anti-GroES and anti-MprB antibodies were used to detect control proteins. Fraction abbreviations: Cyt, cytosol; M, membrane; LD, lipid droplets. Hydrophobicity (H) and mean hydrophobic moment (μH) values are noted for each H1 domain. The images shown are representative of experiments performed in triplicate.

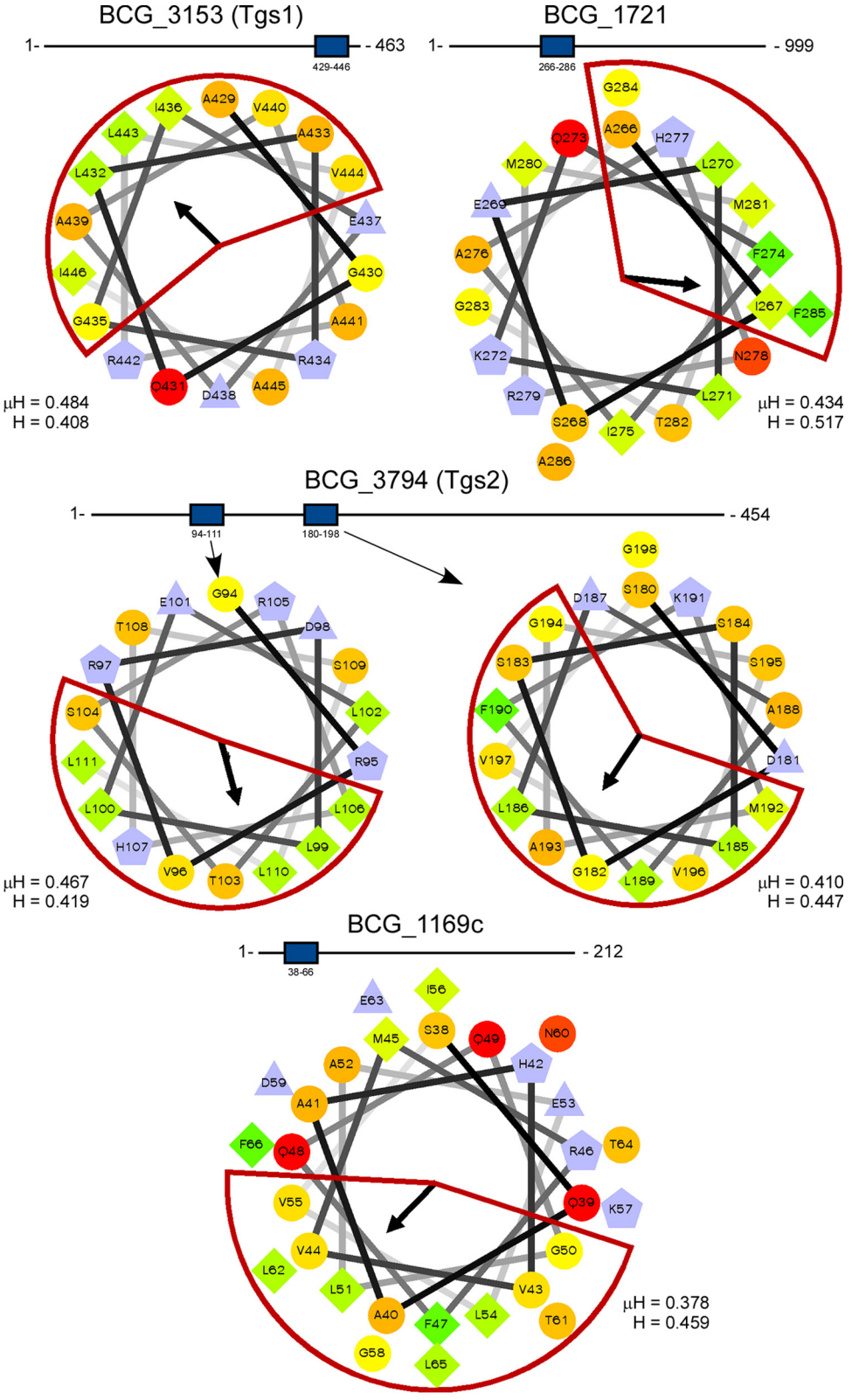

FIG 5 LD-associated proteins from *M. bovis* BCG possess amphipathic helices. Amphipathic helices were identified in BCG_3153 (Tgs1), BCG_1721, BCG_3794 (Tgs2), and BCG_1169c (18) using Heliquest. The length of each protein is shown. The location of amphipathic helices within each sequence is denoted by a blue box. The hydrophobic face of each helix is highlighted in red. The mean hydrophobic moment (μH) and hydrophobicity (H) values are noted. The arrows indicate the angles of the mean hydrophobic moments.

TABLE 1 Fifty most abundant proteins in the *M. smegmatis* LD proteome based on label-free quantification

UniProt accession no.	Gene	Protein	No. of unique peptides	% coverage	Avg LFQ
Q3I5Q7	MSMEG_0919	HBHA-like protein	38	69.4	2.14E+09
A0QVU2	MSMEG_2695	35-kDa protein	36	97.1	1.99E+09
A0R5R3	MSMEG_6282	KanY protein	18	95.2	8.81E+08
A0QR91	MSMEG_1030	4-Hydroxyacetophenone monooxygenase	50	86.8	7.22E+08
A0R2B0	MSMEG_5048	Membrane protein	17	60.1	4.45E+08
A0QPE8	*fadA2*	3-Ketoacyl coenzyme A thiolase	27	78.5	3.91E+08
A0R535	MSMEG_6049	Secreted protein	19	75.8	3.77E+08
A0QPE7	*fabG*	3-Ketoacyl-ACP reductase	44	96	2.88E+08
A0QQU5	*groL1*	60-kDa chaperonin 1	44	82.4	2.31E+08
A0QRD5	MSMEG_1077	Deazaflavin-dependent nitroreductase family protein	19	88.6	2.23E+08
A0QSD7	*rpsC*	30S ribosomal protein S3	35	80	2.15E+08
A0QNM6	MSMEG_0098	Methyltransferase	19	83.5	2.05E+08
A0QZX9	MSMEG_4188	Short-chain dehydrogenase	29	91.5	2.02E+08
Q9ZHC5	*hup*	DNA-binding protein HU homolog	13	39.4	1.92E+08
A0QQS8	MSMEG_0863	Short-chain dehydrogenase	23	74.3	1.57E+08
A0QYS3	MSMEG_3767	Acyl coenzyme A synthase	57	76.5	1.53E+08
A0R200	*atpD*	ATP synthase subunit beta	33	90.7	1.52E+08
A0R5I8	MSMEG_6207	Polyketide cyclase	18	80.6	1.50E+08
A0QWW2	gapA	Glyceraldehyde-3-phosphate dehydrogenase	18	68.2	1.47E+08
A0R1E4	MSMEG_4722	Short-chain dehydrogenase	27	93.7	1.40E+08
A0QSE0	*rpsQ*	30S ribosomal protein S17	19	87.8	1.38E+08
A0R0W7	MSMEG_4533	Sulfate ABC transporter substrate-binding protein	17	66.8	1.28E+08
A0QR89	MSMEG_1028	Geranylgeranyl reductase	30	79.5	1.28E+08
A0QR11	MSMEG_0946	NAD-dependent epimerase/dehydratase family protein	26	76.9	1.25E+08
A0QW19	*dxs*	1-Deoxy-D-xylulose-5-phosphate synthase	43	89	1.22E+08
A0QQ49	MSMEG_0625	Peptidase	21	66.4	1.22E+08
A0R3D1	MSMEG_5430	Oxidoreductase	18	85.9	1.15E+08
A0QX80	MSMEG_3204	Uncharacterized protein	13	73	1.13E+08
A0QTV7	MSMEG_1981	Nitroreductase	14	75.3	1.09E+08
A0R157	MSMEG_4632	Enoyl reductase	35	91.6	1.03E+08
A0R723	MSMEG_6753	Oxidoreductase, short-chain dehydrogenase/reductase family protein	17	75.4	1.01E+08
A0QNZ7	MSMEG_0220	Monoglyceride lipase	18	87.5	9.79E+07
A0QNF5	*cwsA*	Cell wall synthesis protein CwsA	6	57.4	9.72E+07
A0QPJ9	MSMEG_0424	Hsp20/alpha crystallin family protein	18	84.8	9.70E+07
A0R5S1	MSMEG_6291	Amino acid dehydrogenase	25	74.8	9.55E+07
A0R058	*asnB*	Asparagine synthetase	39	73.3	9.35E+07
A0QS97	*rpsG*	30S ribosomal protein S7	15	71.2	9.15E+07
A0QTL0	MSMEG_1882	Acyltransferase, ws/dgat/mgat subfamily protein	41	88.5	8.98E+07
A0QXG0	MSMEG_3287	Alpha/beta hydrolase	17	68.3	8.96E+07
A0R202	*atpA*	ATP synthase subunit alpha	34	65.5	8.53E+07
A0QSZ3	*icd2*	Isocitrate dehydrogenase	40	66.1	8.36E+07
A0QQY3	MSMEG_0918	Transcriptional regulator, XRE family	14	97.2	8.17E+07
A0R073	MSMEG_4284	Multidrug MFS transporter	14	69.9	8.16E+07
A0QS66	*rpoC*	DNA-directed RNA polymerase subunit beta	87	76.8	8.12E+07
A0QS98	*tuf*	Elongation factor Tu	25	86.4	7.90E+07
A0R2S3	MSMEG_5215	Nitroreductase	12	75.6	7.90E+07
A0R5H6	MSMEG_6195	Anion transporter	25	67.8	7.82E+07
A0QPG9	MSMEG_0394	Uncharacterized protein	11	100	7.61E+07
A0QR12	MSMEG_0947	Acyltransferase	21	74.3	7.50E+07
A0QPG2	MSMEG_0387	Rmt2 protein	16	79.5	7.13E+07

were designated as being LD associated. In total, 480 proteins (~7% of the *M. smegmatis* proteome) satisfied these criteria (see Table S3). This is similar to the number of LD proteins reported in *Rhodococcus jostii* RHA1 (16). The 50 top scoring hits from this analysis based on relative protein abundance (average label-free quantification [LFQ]) are shown in Table 1. The identified proteins are predicted to possess diverse biological functions, including biosynthesis, metabolism, protein folding, replication, transcription, and translation. Of note, MSMEG_2695 (PspA), was the second most abundant protein observed on LDs (Table 1). Interestingly, the most abundant protein was MSMEG_0919, a homolog of the heparin-binding hemagglutinin (HbhA) from *M. tuberculosis* (Table 1) (40). HbhA is an established surface-exposed adhesion and a

multifunctional virulence determinant (41–46). MSMEG_0919 is also orthologous to *Rhodococcus* microorganism lipid droplet small (MLDS), an LD-associated protein that regulates LD size and content (16). In addition, this protein binds to genomic DNA on the surface of LDs, and enhances the protection against genotoxic stress encountered by *Rhodococcus* (47). Of the 480 proteins identified by LC-MS/MS, 26 (~5%) were also identified in the Heliquest search as possessing one or more amphipathic helices with characteristics similar to the $PspA_{Mtb}$ H1 domain (Table 2). Several of these proteins are predicted to be involved in metabolic processes (Table 2), while others regulate the processes of transcription, translation, and protein degradation (Table 2). Thus, *M. smegmatis* harbors a total of 22 proteins that possess H1-like amphipathic helices similar to that in $PspA_{Mtb}$ and that localize to the surface of LDs.

Finally, to validate the results from computational and LC-MS/MS analyses, the DNA sequence encoding the amphipathic helix present in MSMEG_4703 (residues 212 to 229) (Table 2) (Fig. 6A) was synthesized and cloned in front of GFPmut3. This helix has μH and H values of 0.545 and 0.539, respectively (Fig. 6B). Importantly, there are six large hydrophobic residues on the hydrophobic face of this helix (Fig. 6B). Following construction, the resulting plasmid was introduced into *M. smegmatis* Δ*pspA*, and the localization of the chimeric GFPmut3 variant was assessed as described previously. While GFPmut3 localized exclusively to the cytoplasmic compartment (data not shown), the MSMEG_4703 (212 to 229) GFPmut3 chimera was observed in multiple fractions, including the LD compartment (Fig. 6C). In contrast, GroES and MprB were observed in the cytoplasmic and membrane compartments, respectively, confirming the fractionation procedure (Fig. 6C). In summary, the *M. smegmatis* proteome includes proteins predicted to contain one or more $PspA_{Mtb}$ H1-like amphipathic helices. Furthermore, a subset of these proteins is present on *M. smegmatis* LDs, possibly through interactions facilitated by one or more amphipathic helices.

DISCUSSION

LDs are unique in biology as they represent the only naturally occurring structures utilizing a phospholipid monolayer to separate organic from aqueous phases. Nearly all eukaryotic cells are able to produce LDs, and as a result, much is known about their structure and function within these hosts. However, LD production in bacteria is much less common, and our understanding of prokaryotic LDs is still in its infancy. Recent studies from our laboratory have identified phage shock protein PspA as a constituent of LDs produced by *Mycobacterium* spp., including *M. tuberculosis* and *M. smegmatis* (17). The deletion or overproduction of PspA in these organisms alters the size distribution of LDs and negatively impacts bacterial survival in an *in vitro* culture model of nonreplicating persistence (17). To begin elucidating the properties of prokaryotic LDs, PspA proteins from *M. tuberculosis* and an *M. smegmatis* Δ*pspA* surrogate host were used as model systems to (i) begin defining the mechanism by which PspA localizes to *Mycobacterium* LDs and (ii) determine if other *Mycobacterium* proteins associate with LDs using a similar mechanism. The use of *M. smegmatis* Δ*pspA* for these studies was advantageous for several reasons. The isolation of LDs requires the use of aerosol-generating equipment not currently available in our biosafety level 3 laboratory, precluding the use of *M. tuberculosis* as an LD source. Furthermore, the production of proteins in the Δ*pspA* mutant background enabled the study of protein-LD interactions independent of interactions between endogenous PspA and cloned PspA variants.

The $PspA_{Mtb}$ H1 domain contains 6 large hydrophobic residues (F5, W9, L12, M13, F16, and I20) along the hydrophobic face of the helix and five charged residues (K7, K10, K19, D21, E22) on the hydrophilic face of the helix, resulting in a net charge of +1. The removal of the H1 domain completely abrogated the binding of $PspA_{Mtb}$ to LDs. Similarly, cloning of the H1 domain to the N terminus of GFP enabled this otherwise cytoplasmic protein to associate with LDs. An amphipathic helix is present in the N terminus of most if not all PspA/Vipp1 family members that have been characterized to date. Although the N-terminal amphipathic helix present in *E. coli* PspA (AHa, residues 2 to 19) shares no sequence homology with the $PspA_{Mtb}$ H1 domain, $PspA_{Eco}$ is capable

TABLE 2 *M. smegmatis* LD proteins possessing amphipathic helices like the $PspA_{Mtb}$ H1 domain

UniProt accession no.	Gene	Protein	No. of unique peptides	% coverage	Avg LFQ	Helix position	Helix sequence
A0QVU2	MSMEG_2695	35-kDa protein	36	97.1	1.99E+09	5–23	FVKAWKYLMALFSSKVDEY
A0QWW2	*gapA*	Glyceraldehyde-3-phosphate dehydrogenase	18	68.2	1.47E+08	167–185	LAKVLNDEFGIVKGLMTTI
A0QS66	*rpoC*	DNA-directed RNA polymerase subunit beta	87	76.8	8.12E+07	835–852	IKSSFREGLTVLEYFINT
A0R2B1	*kgd*	Multifunctional 2-oxoglutarate metabolism enzyme	55	60.4	4.89E+07	972–989	LWEAQFGDFVNGAQSIID
A0R203	*atpFH*	ATP synthase subunit b-delta	31	67.4	4.86E+07	198–215	GLTNLADELASVAKLLLS
A0QV46	MSMEG_2444	Dienelactone hydrolase family protein	11	51.3	3.85E+07	211–228	AATTDAWTRVFAFFDEHL
A0QSD8	*rplP*	50S ribosomal protein L16	8	62.3	3.50E+07	52–69	IAINRHIKRGGKVWINIF
A0R6J9	MSMEG_6575	Beta-lactamase	22	73.8	3.11E+07	28–45	RAIEQIWDSVRYWYQSGL
A0R7C5	MSMEG_6859	Oxidoreductase	15	87.6	1.57E+07	106–123	LADWHRTIDVNIGGVLNV
A0QW02	*sigA*	RNA polymerase sigma factor SigA	17	38.4	1.21E+07	390–407	SFTLLQDQLQSVLETLSE
A0QT91	MSMEG_1757	DEAD/DEAH box helicase	31	30.5	9.42E+06	1193–1210	ILETLGHGGAYFFRQLTD
A0R3M4	*sucC*	Succinate coenzyme A ligase (ADP-forming) subunit beta	12	37.2	8.63E+06	166–183	LDAAAVTIQKLWEVFVKE
A0R2B5	MSMEG_5053	Acetoin dehydrogenase	18	74.1	5.88E+06	247–264	KILDVIVRITGSGYQRLF
A0R564	*disA*	DNA integrity scanning protein DisA	11	37.6	5.71E+06	346–364	GIGSMWARHIREGLSLLAE
A0R564	*disA*	DNA integrity scanning protein DisA	11	37.6	5.71E+06	318–337	AHVDLLVRSFGSLQNLLAAS
A0R5R4	MSMEG_6283	FAD-binding domain protein	16	51.5	5.40E+06	185–202	FHSITDLVAAMDRIIETG
A0QNJ7	MSMEG_0067	Conserved hypothetical proline and alanine rich protein	13	43.7	4.66E+06	348–365	GLFQKATRGVLSTISGLV
A0QS46	*rplA*	50S ribosomal protein L1	8	44.3	4.20E+06	94–117	IVGSDDLIEKIQGGFLDFDAAIAT
A0R574	*clpC1*	ATP-dependent Clp protease, ATP-binding subunit ClpC1	20	38.2	3.67E+06	725–743	DEIIQMVDLMIGRVSNQLK
A0R1C6	MSMEG_4703	Glycerol-3-phosphate acyltransferase	21	42.2	3.04E+06	212–229	EMLDELSTGWSRFSVDLI
A0QT70	MSMEG_1736	Glycerol-3-phosphate dehydrogenase	12	32.4	2.82E+06	443–462	VRHLLDRYGSLIGEVLALAD
A0QTW2	MSMEG_1986	Tartrate dehydrogenase	9	27.3	2.73E+06	88–105	SLWGSLIQFRRHFDQYVN
A0QVM7	*infB*	Translation initiation factor IF-2	10	25.6	2.68E+06	491–508	SVIYQAIDEIEAALKGML
A0R730	MSMEG_6761	Glycerol-3-phosphate dehydrogenase	12	28.2	2.11E+06	435–452	VAHLLGRYGTLTDELLEI
A0QRV5	MSMEG_1252	Uncharacterized protein	28	21.9	2.01E+06	1374–1391	GMSVRALMDNFGELITQI
A0QWV7	MSMEG_3079	Nucleotide-binding protein MSMEG_3079/MSMEI_3001	8	40.9	1.57E+06	222–240	GALEFLDTYHRLLDVVIDG
A0R4M2	MSMEG_5884	3-Hydroxyisobutyrate dehydrogenase family protein	5	34.4	9.87E+05	181–198	IASVIESLGEAMALVGKA

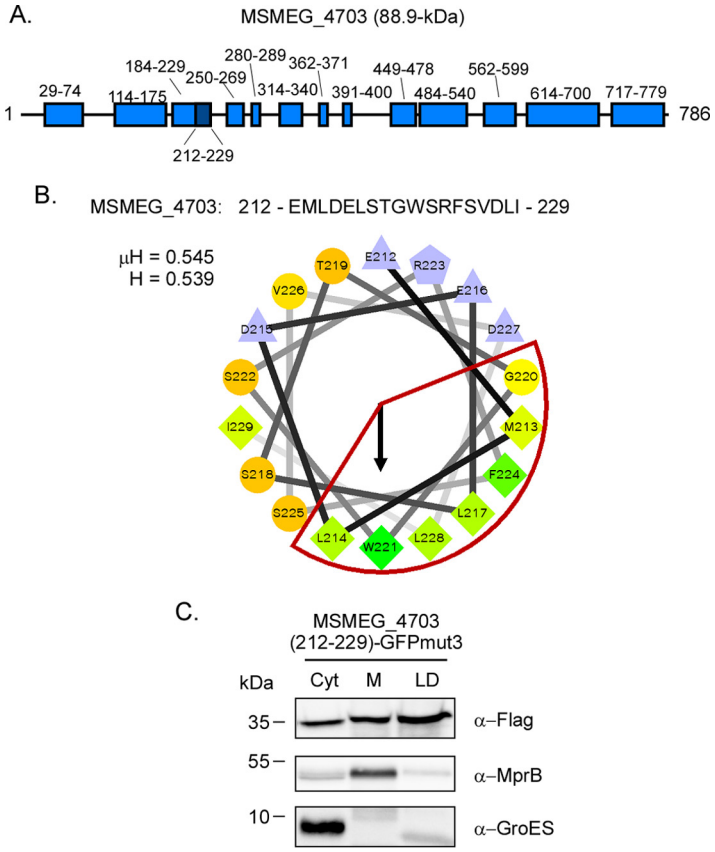

FIG 6 The amphipathic helix from MSMEG_4703 targets GFPmut3 to lipid droplets. (A) Schematic of Psipred-predicted helices of MSMEG_4703. Light blue boxes denote the location of α-helical domains, and the dark blue box denotes the location of the amphipathic helix identified using Heliquest. (B) The amino acid sequence of the amphipathic helix (residues 212 to 229) and the helical wheel diagram of residues 212 to 229. The hydrophobic face of the amphipathic helix is highlighted in red. Hydrophobicity (H) and mean hydrophobic moment (μH) values are noted. The arrow indicates the angle of the mean hydrophobic moment. (C) Western blot showing localization of 3×Flag-MSMEG_4703 (212 to 229) GFPmut3 following production in *M. smegmatis* Δ*pspA*. $PspA_{Eco}$ was detected using anti-Flag antibody. Anti-GroES and anti-MprB antibodies were used to detect control proteins. Fraction abbreviations: Cyt, cytosol; M, membrane; LD, lipid droplets. The images shown are representative of experiments performed in triplicate.

of associating with LDs when produced in *M. smegmatis*. Interestingly, only a minor fraction of $PspA_{Eco}$ associates with membranes, a predominant site of localization for this protein when produced endogenously in *E. coli*. While the reasons for this discrepancy are currently unclear, we speculate that the lipid surface area of LDs far exceeds that of the plasma membrane under the conditions utilized in these studies. Alternatively, or in addition to, LDs are expected to possess a much higher stored curvature elastic stress (see below) compared to that of the plasma membrane of unstressed bacteria. In contrast to that of $PspA_{Eco}$, the H1 domain of $PspA_{Rho}$ differs by only two residues from the H1 domain of $PspA_{Mtb}$ (L12M and S17N). $PspA_{Rho}$ binds LDs when produced in its natural host (16) but is also capable of binding LDs when produced in *M. smegmatis*. While it remains unclear whether the N-terminal amphipathic helices present in $PspA_{Eco}$ and $PspA_{Rho}$ facilitate their association to LDs, $PspA_{Eco}$ variants lacking AHa are deficient in their ability to bind lipids (23, 31, 48). Furthermore, fusion of the AHa domain to the N terminus of GFP promotes the association of this protein with lipid membranes (23). Thus, the N-terminal amphipathic helix present in $PspA_{Mtb}$, and possibly other PspA family members, regulates the binding to *Mycobacterium* LDs.

Amphipathic helices are a common motif of proteins that interact with lipid membranes. However, amphipathic helices are also an established mechanism by which

cytoplasmic proteins associate with the lipid monolayer of LDs produced in eukaryotes (32–36). A recent study indicates that the most important characteristic for an amphipathic helix to bind LDs is the number of large hydrophobic residues (I, F, L, M, W, and Y) that are present on the hydrophobic face of the helix (35). In particular, LD binding is most frequently observed with amphipathic helices possessing at least 5 large hydrophobic residues, with the amount of binding proportional to the number of large hydrophobic residues present (35). In contrast, little if any correlation is observed between LD binding and the net charge or hydrophobic moment of the amphipathic helix (35). The N-terminal amphipathic helices present in $PspA_{Mtb}$, $PspA_{Eco}$, and $PspA_{Rho}$ each possess 5 or more large hydrophobic residues along their hydrophobic faces. Interestingly, $PspA_{Mtb}$ double and triple mutants (F5A/W9A, F5A/F16A, W9A/F16A, and F5A/W9A/F16A) that harbor only 4 or 3 large hydrophobic residues on the hydrophobic face of the H1 helix remain able to bind *Mycobacterium* LDs. This phenotype is conserved when H1 mutant variants are cloned in front of GFPmut3. Therefore, H1 binding to LDs occurs independently of $PspA_{Mtb}$ oligomerization and is able to proceed with only a limited number of large hydrophobic residues relative to other amphipathic helices shown to bind LDs. Interestingly, additional residues along the hydrophilic face of the H1 domain may also contribute to LD binding by $PspA_{Mtb}$. For example, the $PspA_{Mtb}$ K7A mutant is reduced in its ability to bind *Mycobacterium* LDs. A substitution at this residue alters the net charge of the helix from $+1$ to neutral. Therefore, the K7A substitution may impact LD binding by altering electrostatic interactions between the hydrophilic face of the H1 domain and the negatively charged phospholipids of the LD monolayer. Regardless, our results indicate that the properties of $PspA_{Mtb}$ important for its ability to bind LDs are complex and multifaceted and may include interactions that require both faces of the H1 amphipathic helix.

In addition to the H1 amphipathic helix, the ability of PspA family members to bind *Mycobacterium* LDs may also be related to one or more general characteristics of the phospholipid monolayer surrounding LDs. The H1 domains of PspA and Vipp1 exhibit high affinities for membranes possessing lipid-packing defects (i.e., membranes exhibiting stored curvature elastic [SCE] stress) (23, 24). The spherical conformation of LDs by their very nature induces SCE stress within the phospholipid monolayer due to the space restrictions placed on acyl chains (49). In addition, the neutral lipid core of LDs pokes into the phospholipid monolayer and imparts additional packing defects on the phospholipid acyl chains comprising the LD monolayer (35). Apart from inherent SCE stress, the negatively charged head groups present on the LD phospholipid monolayer are also known to mediate interactions with PspA and Vipp1 (23, 24). As the phospholipid monolayer of bacterial LDs is thought to be derived from the plasma membrane, the *M. smegmatis* LD phospholipid monolayer is expected to contain several negatively charged lipid species, including phosphatidic acid, phosphatidylserine, phosphatidylglycerol, cardiolipin, and various phosphatidylinositol species (50–52). Thus, the presence of anionic phospholipids and the general lipid packing defects present within the phospholipid monolayer may regulate the localization of PspA family members to LDs.

Apart from $PspA_{Mtb}$, other *Mycobacterium* proteins may also associate with LDs via amphipathic helices. For example, several of the proteins present on *M. bovis* BCG LDs contain one or more amphipathic helices with characteristics similar to $PspA_{Mtb}$ (18). Furthermore, of the $>$6,000 proteins predicted to be encoded by the *M. smegmatis* genome, 330 of these proteins possess $PspA_{Mtb}$-like amphipathic helices that contain five or more large hydrophobic residues along the hydrophobic face. Finally, LC-MS/MS analyses identified a total of $\sim$480 proteins that are present on LDs isolated from *M. smegmatis*, and 26 of these possess amphipathic helices similar to the $PspA_{Mtb}$ H1 domain. One of these proteins, MSMEG_4703, is a predicted glycerol-3-phosphate acyltransferase. This enzyme functions in the first of two committed steps in the synthesis of phosphatidic acid, a precursor needed to produce both triacylglycerol and anionic phospholipids (53, 54). Cloning of the identified amphipathic helix from MSMEG_4703 (residues 212 to 229) in front of GFPmut3 alters the localization pattern of this protein to now include LDs. The *M. tuberculosis* homolog of this protein (Rv1551)

also contains an amphipathic helix in the same region that differs by only 4 residues from MSMEG_4703 (data not shown). The expression of *Rv1551* in *E. coli* leads to higher levels of several glycerophospholipids within the cell, including phosphatidylglycerol, phosphatidylethanolamine, and cardiolipin (55). Thus, MSMEG_4703/Rv1551 is likely to regulate several aspects of LD biology in *Mycobacterium*. In addition to MSMEG_4703, several other LD-associated proteins that possess $PspA_{Mtb}$-like amphipathic helices may also regulate the synthesis or metabolism of LDs. These include two predicted glycerol-3-phosphate dehydrogenases (MSMEG_1736/GlpD2 and MSMEG_6761), which are involved in the conversion of glycerol-3-phosphate to dihydroxyacetone and vice versa (56), and glyceraldehyde-3-phosphate dehydrogenase (MSMEG_3084/GapA), which mediates the reversible conversion of glyceraldhehyde-3-phosphate to 3-phospho-D-glyceroyl phosphate. Interestingly, orthologs of these three enzymes have also been identified on LDs produced by *R. jostii* RHA1 (16), indicating that they, along with PspA and HbhA, may represent part of the core proteome of LDs produced in bacteria.

In summary, our understanding of prokaryotic LDs remains in its infancy. The work described here extends our limited knowledge of these quasi-organelles by defining the proteomic composition of LDs produced in *M. smegmatis* and by identifying a key structural motif that facilitates the interaction of PspA, as well as other proteins, with LDs produced in *Mycobacterium*. Going forward, this information may help in the development of novel therapeutics capable of disrupting key LD-protein interactions needed by *M. tuberculosis* for survival during nonreplicating persistence.

MATERIALS AND METHODS

Bacterial strains, media, and culture conditions. The strains and plasmids used in this study are described in Table 3. *Escherichia coli* strains DH5α, Top10, (Thermo Fisher Scientific, Waltham, MA), and NovaBlue (MilliporeSigma, Burlington, MA) were used for cloning. Protein purification was carried out in *E. coil* strain BL21(DE3) containing plasmid pLysS. All *E. coli* strains were incubated at 37°C in Luria-Bertani (LB) medium with 100 μg/ml ampicillin, 50 μg/ml kanamycin, 150 μg/ml hygromycin B, and/or 25 μg/ml chloramphenicol for selection, as necessary. *Rhodococcus jostii* strain RHA1 was kindly provided by Lindsay Eltis (University of British Columbia, Canada) and was cultured at 30°C in LB medium. All *Mycobacterium* strains are from American Type Culture Collection (ATCC; Manassas, VA) and are derivatives of *Mycobacterium tuberculosis* H37Rv (ATCC 27294) or *Mycobacterium smegmatis* mc^2155 (ATCC 700084). For general culturing, mycobacteria were incubated at 37°C in Middlebrook 7H9 broth (BD, Franklin Lakes, NJ) with shaking or on Middlebrook 7H10 agar (BD, Franklin Lakes, NJ). Broth and agar media were supplemented with 0.5% glycerol (MilliporeSigma, Burlington, MA), 0.05% Tween 80 (Sigma, St. Louis, MO), and either 10% albumin-dextrose-catalase (ADC; *M. smegmatis*) or 10% oleic acid-albumin-dextrose-catalase (OADC; *M. tuberculosis*) (BD, Franklin Lakes, NJ). Mycobacteria were also grown in Sauton's medium (57) at 37°C for 7 days to induce LD production. When needed, *Mycobacterium* medium was supplemented with 50 μg/ml hygromycin B.

Construction of plasmids. Primers used in this study are described in Table S1 in the supplemental material and were synthesized by Eurofins Genomic (Louisville, KY). To generate expression constructs, the coding sequences from genes of interest were first amplified by PCR with Platinum *Pfx* (Thermo Fisher Scientific, Waltham, MA) using primer sets containing engineered restriction endonuclease recognition sequences. Amplified products were then cloned into pCR2.1-TOPO (Thermo Fisher Scientific, Waltham, MA) or pSTBlue-1 (MilliporeSigma, Burlington, MA), and cloned DNA was confirmed by sequencing (MCLAB, San Francisco, CA). The resulting constructs were then digested with the appropriate restriction enzyme(s), and the released product of interest was subcloned into an *E. coli* or *Mycobacterium* expression vector. pTZ1227 has been described previously and was the vector used to produce 3×Flag-$PspA_{Mtb}$-6×His in *Mycobacterium* (17). $PspA_{Mtb}$ΔH1 was generated by amplifying *M. tuberculosis* genomic DNA using primers 2744c_H1FWDNheI and 2744cRev4-NotI. This variant lacks the first 22 amino acids of $PspA_{Mtb}$, which includes the H1 domain. The resulting product was subcloned into pTZ842 (58) to allow incorporation of a 3×Flag epitope at the N terminus and a 6×His epitope tag at the C terminus of $PspA_{Mtb}$ΔH1, resulting in pTZ1490. The sequence encoding 3×Flag-$PspA_{Mtb}$ΔH1-6×His was then amplified from pTZ1490 using the primers Rv2744cFpSE100PstI and 2744cRpSE100EcoRV, and the resulting product was subcloned into pSE100 for expression in *Mycobacterium* (59), resulting in pTZ1494. pTZ1168 was used to produce $PspA_{Mtb}$-His in *E. coli* and has been described previously (58). To produce $PspA_{Mtb}$ΔH1-His in *E. coli*, the sequence encoding $PspA_{Mtb}$ΔH1 was amplified from *M. tuberculosis* H37Rv genomic DNA using primers 2744c_H1FWDNheI and 2744cRev4-NotI and subcloned into pET24b (EMD Millipore, Burlington, MA), resulting in pTZ1445. The GFPmut3 coding sequence was generated by amplifying pMV261-*gfpmut3* plasmid DNA (kindly provided by Eric Rubin, Harvard Medical School, Boston, MA) with primers GFPmut3_no_fusion_F and GFPmut3_both_R. The resulting product was then subcloned into pTZ1167, a derivative of pSE100 that carries the coding sequences for 3×Flag and 6×His flanking the multiple cloning site (58), resulting in pTZ1509. To generate chimeras in which the H1 domain from $PspA_{Mtb}$ was fused to GFP, *gfpmut3* was amplified from pMV261-*gfpmut3* plasmid DNA using primers GFPmut3_fusion_F and GFPmut3_both_R. The resulting product was then subcloned

TABLE 3 Strains and plasmids

Strain or plasmid	Genotype or description[a]	Reference or source
Strains		
E. coli DH5α	F$^-$ ϕ80*lacZ*ΔM15 Δ(*lacZYA-argF*)*U169 recA1 endA1 hsdR17*(r_K^- m_K^+) *phoA supE44* λ *thi-1 byrA96 relA1*	Lab collection
E. coli TOP10	F$^-$ *mcrA* Δ(*mrr-hsdRMS-mcrBC*) ϕ80*lacZ*ΔM15 Δ*lacX74 recA1 araD139* Δ*(ara-leu)7697 galU galK rpsL str endA1 nupG*	Lab collection
E. coli BL21(DE3)pLysS	F$^-$ *ompT hsdSB*(r_B^- m_B^-) *gal dcm* (DE3); contains pLysS	Lab collection
E. coli NovaBlue Singles	*endA1 hsdR17*(r_{K12}^- m_{K12}^+) *supE44 thi-1 recA1 gyrA96 relA1 lac* F′[*proA*$^+$*B*$^+$ *lacI*^{q}*Z*ΔM15::Tn*10*] (Tet^r)	Novagen
Rhodococcus jostii RHA1	Laboratory strain	Gift of Eltis lab
M. smegmatis mc^{2}155	Laboratory strain	ATCC 700084
M. tuberculosis H37Rv	Laboratory strain	ATCC 27294
TCZ2054	*M. smegmatis* ΔMSMEG_2695 (Δ*pspA*)	17
TCZ2365	*M. smegmatis* ΔMSMEG_2695 (Δ*pspA*) containing pTZ1227	17
TCZ2547	*E. coli* BL21(DE3) with pLysS containing pTZ1445	This study
TCZ2632	*M. smegmatis* ΔMSMEG_2695 (Δ*pspA*) containing pTZ1477	This study
TCZ2634	*M. smegmatis* ΔMSMEG_2695 (Δ*pspA*) containing pTZ1479	This study
TCZ2642	*E. coli* BL21(DE3) with pLysS containing pTZ1482	This study
TCZ2646	*E. coli* BL21(DE3) with pLysS containing pTZ1484	This study
TCZ2664	*M. smegmatis* ΔMSMEG_2695 (Δ*pspA*) containing pTZ1494	This study
TCZ2729	*M. smegmatis* ΔMSMEG_2695 (Δ*pspA*) containing pTZ1509	This study
TCZ2731	*M. smegmatis* ΔMSMEG_2695 (Δ*pspA*) containing pTZ1511	This study
TCZ2758	*M. smegmatis* ΔMSMEG_2695 (Δ*pspA*) containing pTZ1534	This study
TCZ2783	*M. smegmatis* Δ*MSMEG_2695* (Δ*pspA*) containing pTZ1535	This study
TCZ2784	*M. smegmatis* ΔMSMEG_2695 (Δ*pspA*) containing pTZ1536	This study
TCZ2785	*M. smegmatis* ΔMSMEG_2695 (Δ*pspA*) containing pTZ1537	This study
TCZ2786	*M. smegmatis* ΔMSMEG_2695 (Δ*pspA*) containing pTZ1545	This study
TCZ2787	*M. smegmatis* ΔMSMEG_2695 (Δ*pspA*) containing pTZ1546	This study
TCZ2788	*M. smegmatis* ΔMSMEG_2695 (Δ*pspA*) containing pTZ1547	This study
TCZ2789	*M. smegmatis* ΔMSMEG_2695 (Δ*pspA*) containing pTZ1548	This study
TCZ2790	*M. smegmatis* ΔMSMEG_2695 (Δ*pspA*) containing pTZ1549	This study
TCZ2794	*M. smegmatis* ΔMSMEG_2695 (Δ*pspA*) containing pTZ1550	This study
TCZ2800	*M. smegmatis* ΔMSMEG_2695 (Δ*pspA*) containing pTZ1551	This study
TCZ2801	*M. smegmatis* ΔMSMEG_2695 (Δ*pspA*) containing pTZ1552	This study
TCZ2804	*M. smegmatis* ΔMSMEG_2695 (Δ*pspA*) containing pTZ1555	This study
TCZ2811	*M. smegmatis* ΔMSMEG_2695 (Δ*pspA*) containing pTZ1561	This study
Plasmids		
pCR2.1-TOPO	3.9-kb plasmid for cloning PCR products; Amp^r Kan^r	Invitrogen
pSTBlue1	3.8-kb plasmid for cloning PCR products; Amp^r Kan^r	Novagen
pSE100	TetR-regulated protein expression vector, Hyg^r	59
pET24b	5.3-kb plasmid for expression in *E. coli*, Kan^r	Novagen
pTZ842	pET24b cloning plasmid with 5′ 3×Flag inserted	58
pTZ1160	pSE100 containing 3×Flag-6×His tags flanking the multiple cloning site; Hyg^r	This study
pTZ1167	pSE100 containing 3×Flag-6×His tags flanking the multiple cloning site, altered cutsites from pTZ1160; Hyg^r	58
pTZ1168	pET-24b containing Rv2744c coding sequence; Kan^r	58
pTZ1227	pTZ1167 containing Rv2744c (*pspA*) coding sequence; Hyg^r	17
pTZ1445	pET24b expression vector containing $pspA_{Mtb}$ΔH1	This study
pTZ1477	pTZ1167 containing *pspA* coding sequence from *E. coli* BL21; Hyg^r	This study
pTZ1479	pTZ1167 containing *pspA* coding sequence from *Rhodococcus* RHA1; Hyg^r	This study
pTZ1482	pET24b containing $pspA_{Eco}$	This study
pTZ1484	pET24b containing $pspA_{Rho}$	This study
pTZ1490	$pspA_{Mtb}$ΔH1 inserted into pTZ842 for addition of 5′ 3×Flag and 3′ 6×His tags	This study
pTZ1494	3×Flag-$pspA_{Mtb}$ΔH1-6×His from pTZ1490 inserted into pSE100	This study
pTZ1509	pTZ1167 containing GFPmut3 coding sequence; Hyg^r	This study
pTZ1510	pTZ1167 containing GFPmut3 in-frame for insertion of amphipathic helix	This study
pTZ1511	pTZ1167 containing 3× H1-tagged GFPmut3 coding sequence; Hyg^r	This study
pTZ1514	pTZ1167 containing HbhA from *M. smegmatis* (MSMEG_0919)	This study
pTZ1526	pCR2.1 TOPO containing Rv2744c w/NheI and BglII cutsites for mutagenesis/insertion into pTZ1160	This study
pTZ1534	pTZ1160 containing Rv2744c (*pspA*) F5A mutant coding sequence; Hyg^r	This study
pTZ1535	pTZ1160 containing Rv2744c (*pspA*) W9A mutant coding sequence; Hyg^r	This study
pTZ1536	pTZ1160 containing Rv2744c (*pspA*) F5A/W9A double mutant coding sequence; Hyg^r	This study
pTZ1537	pTZ1160 containing Rv2744c (*pspA*) F16A mutant coding sequence; Hyg^r	This study

(Continued on next page)

TABLE 3 (Continued)

Strain or plasmid	Genotype or description[a]	Reference or source
pTZ1539	pCR2.1-TOPO containing PspA H1 domain fused to GFPmut3	This study
pTZ1545	pTZ1160 containing Rv2744c (*pspA*) F5A/F16A double mutant coding sequence; Hyg^r	This study
pTZ1546	pTZ1160 containing Rv2744c (*pspA*) F5A/W9A/F16A triple mutant coding sequence; Hyg^r	This study
pTZ1547	pTZ1160 containing Rv2744c (*pspA*) W9A/F16A double mutant coding sequence; Hyg^r	This study
pTZ1548	pTZ1160 containing Rv2744c (*pspA*) K7A mutant coding sequence; Hyg^r	This study
pTZ1549	pTZ1160 containing Rv2744c (*pspA*) Y11A mutant coding sequence; Hyg^r	This study
pTZ1550	pTZ1167 containing 1× H1-tagged GFPmut3 coding sequence; Hyg^r	This study
pTZ1551	pTZ1167 containing 1× H1 (W9A) GFPmut3 coding sequence; Hyg^r	This study
pTZ1552	pTZ1167 containing 1× H1 (W9E) GFPmut3 coding sequence; Hyg^r	This study
pTZ1555	pTZ1167 containing MSMEG_4703 (residues 212–229) GFPmut3 coding sequence; Hyg^r	This study
pTZ1561	pTZ1167 containing 1× H1 (F5A/W9A/F16A) GFPmut3 coding sequence; Hyg^r	This study

[a]Hyg^r, hygromycin resistance; Tet^r, tetracycline resistance; Kan^r, kanamycin resistance; Amp^r, ampicillin resistance.

into pTZ1167, resulting in pTZ1510. Next, double-stranded DNA encoding three tandemly arranged copies of the H1 domain (the first 22 amino acids of $PspA_{Mtb}$; $H1^1$-$H1^2$-$H1^3$) was chemically synthesized by GeneArt Gene Synthesis (Thermo Fisher Scientific, Waltham, MA). This fragment was designed to incorporate a small linker encoding Ala-Ala-Ser-Ala at the 3′ end of each H1 domain to enhance flexibility. In addition, restriction endonuclease recognition sequences were engineered between and flanking each H1 domain to facilitate downstream cloning procedures. Finally, the fragment encoding 3×H1 was cloned upstream of *gfpmut3* in pTZ1510, resulting in pTZ1511. To generate a GFP chimera in which a single copy of the H1 domain was fused to GFP, pTZ1511 was digested with restriction endonucleases to release the fragment encoding $H1^3$-GFPmut3. The resulting fragment was then amplified with primers H1_trucation_F and GFPmut3_both_R, and the resulting product was subcloned into pTZ1167, producing pTZ1550. To generate the GFP chimera in which the amphipathic helix present in MSMEG_4703 (amino acids 212 to 229) was fused to *gfpmut3*, MSMEG_4703_HelixF and MSEMG_4703_HelixR were phosphorylated with T4 DNA kinase, mixed together, and annealed, and the corresponding product was cloned into pTZ1510, resulting in pTZ1555. To generate $PspA_{Eco}$ for expression in *M. smegmatis*, *E. coli* BL21 chromosomal DNA was amplified with primers F_Eco_pspA_pET24 and R_Eco_pspA_pSE100, and the corresponding product was subcloned into pTZ1167, resulting in pTZ1477. To generate $PspA_{Rho}$ for expression in *M. smegmatis*, *R. jostii* RHA1 chromosomal DNA was amplified with primers F_Rho_pspA_BamHI and R_Rho_pspA_HindIII, and the corresponding product was subcloned into pTZ1167, resulting in pTZ1479. To generate $PspA_{Eco}$-His or $PspA_{Rho}$-His for production in *E. coli*, $pspA_{Eco}$ or $pspA_{Rho}$ was amplified from the chromosomal DNA using primers F_Eco_pspA_pET24 and Eco_R_pET24real or F_Rho_pspA_BamHI and Rho_R_pET24real, respectively. The corresponding products were then subcloned into pET24b, resulting in pTZ1482 ($PspA_{Eco}$-His) and pTZ1484 ($PspA_{Rho}$-His). Amino acid substitutions within the H1 domain were generated by site-directed mutagenesis using the Change-IT multiple mutation site-directed mutagenesis kit according to the manufacturer's instructions. The base plasmids used for these reactions were pTZ1526 and pTZ1539. Mutagenic primers were designed to include 15 to 18 bp of sequence homology flanking the codon(s) targeted for mutagenesis. All primers were synthesized to include a 5′ phosphate. The Amp REV primer provided in the mutagenesis kit was used to synthesize the opposite strand. Mutant variants harboring multiple codon substitutions were generated by sequential mutagenesis. Once mutant alleles were generated and nucleotide changes confirmed, the corresponding sequence was amplified from the vector using Rv2744cFWD-NheI and Rv2744c_Rev_BglII ($PspA_{Mtb}$ variants) or Rv2744cFWD-NheI and GFPmut3_both_R (H1-GFPmut3 variants). The resulting products were then subcloned into pTZ1160 or pTZ1167, respectively. Using this strategy, the following mutant derivatives were generated: pTZ1534 ($PspA_{Mtb}$F5A), pTZ1535 ($PspA_{Mtb}$W9A), pTZ1536 ($PspA_{Mtb}$F5A/W9A), pTZ1537 ($PspA_{Mtb}$F16A), pTZ1545 ($PspA_{Mtb}$F5A/F16A), pTZ1546 ($PspA_{Mtb}$F5A/W9A/F16A), pTZ1547 ($PspA_{Mtb}$W9A/F16A), pTZ1548 ($PspA_{Mtb}$K7A), pTZ1549 ($PspA_{Mtb}$Y11A), pTZ1551 (H1[W9A]-GFPmut3), pTZ1552 (H1[W9E]-GFPmut3), and pTZ1558 (H1[F5A/W9A/F16A]-GFPmut3).

Induction and isolation of *Mycobacterium* lipid droplets. Mid-log-phase cultures of *M. smegmatis* that were grown in 7H9 were washed 3 times in phosphate-buffered saline (PBS) and inoculated in fresh Sauton's medium supplemented with 0.05% Tween 80 at an optical density at 600 nm (OD_{600}) of ~0.1. The cultures were grown for 1 week at 37°C with shaking, and bacteria were harvested by centrifugation. Bacterial pellets were suspended in 20 ml buffer A (25 mM Tricine, 250 mM sucrose [pH 7.8]) containing 1:1,000 protease inhibitor cocktail (Sigma, St. Louis, MO), and were incubated on ice for at least 30 min. Bacteria were lysed by passage 3 times through a French pressure cell, and the lysate was cleared of large debris by centrifugation. Eight milliliters of cleared lysate was then placed in an SW41 ultracentrifuge tube, and 2 ml of buffer B (20 mM HEPES, 100 mM KCl, 2 mM $MgCl_2$ [pH 7.4]) was carefully layered on top. Samples were centrifuged at ~100,000 × *g* for 1 h at 4°C, and LDs were carefully skimmed off the top of the tubes. LDs were washed 3 times in buffer B and stored at −20°C until needed. Cytoplasmic proteins were collected from the middles of the ultracentrifugation tubes and were cleared of contam-

inants via a second ultracentrifugation step at 100,000 × *g* and 4°C. Membrane proteins were collected by suspending the pellets from the initial ultracentrifugation step in buffer B with 0.1% Triton X-100 and agitating overnight at 4°C. Cytoplasmic and membrane proteins were stored at −20°C until needed.

SDS-PAGE and Western blotting. Ten micrograms of total protein was denatured by incubating with 2× SDS loading dye for >10 min at 95°C and resolved by sodium dodecyl sulfate-polyacrylamide gel electrophoresis (SDS-PAGE). Proteins were stained with Coomassie brilliant blue (Thermo Fisher Scientific, Waltham, MA) or were transferred onto polyvinylidene difluoride (PVDF) membrane using the Trans-Blot Turbo transfer system (Bio-Rad, Hercules, CA). For Western blotting, membranes were first blocked in TTBS (20 mM Tris-HCl [pH 7.5], 500 mM NaCl, 0.5% Tween 20) containing 5% skim milk for 1 h and then probed with antiserum diluted in TTBS overnight at 4°C. The primary antibodies used included mouse anti-Flag (1:5,000; Sigma, St. Louis, MO), mouse anti-GroES (1:3,000; BEI Resources, NIAID, NIH), and rabbit anti-MprB (1:3,000; Covance, Denver, PA). Membranes were then washed twice for 5 min each in TBS (20 mM Tris-HCl [pH 7.5], 500 mM NaCl) and three times for 10 min each in TTBS before incubating for 2 h at room temperature with goat anti-mouse IgG (1:5,000; Thermo Fisher Scientific, Waltham, MA) or donkey anti-rabbit IgG (1:1,500) secondary antibody conjugated to horseradish peroxidase. Following washing in TBS and TTBS, the blots were then developed using the SuperSignal West Pico chemiluminescent substrate kit (Thermo Fisher Scientific) and visualized on a ChemiDoc Touch imaging system (Bio-Rad, Hercules, CA).

Production and purification of $PspA_{Mtb}$-His, $PspA_{Mtb}\Delta H1$-His, $PspA_{Eco}$-His, and $PspA_{Rho}$-His. PspA from various bacterial species was produced and purified in *E. coli* using Ni^{2+} affinity chromatography. Briefly, *E. coli* BL21(DE3)pLysS producing PspA-His variants was grown in 1 liter LB medium with selection at 37°C until cells reached mid-exponential phase. Protein expression was then induced by incubation with 1.0 mM IPTG (isopropyl-β-D-thiogalactopyranoside) for 3 h at 37°C. After induction, the cultures were harvested by centrifugation at 8,000 × *g* at 4°C. The bacterial pellet was suspended in 30 ml binding buffer (50 mM Na_2HPO_4 [pH 8.0], 300 mM NaCl, 10 mM imidazole) containing 3 μg/ml DNase, 3 μg/ml RNase, and 30 μl protease inhibitor cocktail (all from Sigma, St. Louis, MO) and lysed by passage through a French pressure cell. The total cell lysate was clarified by centrifugation at 25,000 × *g* for 30 min, rocked with Ni^{2+}-agarose (Qiagen, Venlo, the Netherlands) for 90 min at 4°C, and then processed by batch purification. Bound protein was incubated with binding buffer, followed by incubating twice with wash buffer (50 mM Na_2HPO_4 [pH 8.0], 300 mM NaCl, 25 mM imidazole). Protein was removed by incubating Ni^{2+}-resin sequentially with 1-ml aliquots of elution buffer (50 mM Na_2HPO_4 [pH 8.0], 300 mM NaCl, 150 mM imidazole). The collected fractions were then analyzed by SDS-PAGE. Gels were stained with Coomassie brilliant blue to assess the extent of protein induction and enrichment.

Sucrose gradient ultracentrifugation and negative-stain electron microscopy. The oligomeric status of purified PspA was assessed using sucrose gradient ultracentrifugation. Briefly, 0.5 mg of wild-type PspA, PspA variants, or protein standards (β-amylase, 200 kDa; thyroglobulin, 670 kDa; blue dextran, >2,000 kDa) was loaded onto 10-ml 10 to 50% linear sucrose gradients (Gradient Master; Biocomp Instruments) and resolved using an SW-41 swinging-bucket rotor at 100,000 × *g* for 16 h and 4°C; 0.5-ml aliquots were then removed sequentially from the top of each gradient, and protein content assessed by measuring A_{280}. The fraction containing the largest amount of protein was then used for negative-stain electron microscopy. Fractions were diluted to 100 μg/ml, adsorbed onto ionized copper/Formvar 400 mesh grids, and imaged on a Hitachi H600 transmission electron microscope (TEM) at an accelerating voltage of 75 kV with a magnification from ×100,000 to ×300,000.

Secondary structure predictions and helical wheel analyses. Alpha-helical domains were identified using Psipred (http://bioinf.cs.ucl.ac.uk/psipred/) and other secondary structure prediction algorithms. Helical wheel diagrams were generated using the website http://rzlab.ucr.edu/scripts/wheel/wheel.cgi. Residues were colored from most hydrophobic (green) to least hydrophobic (red), with charged residues colored gray. The mean hydrophobic moment (μH) vector of each helix was represented by an arrow, and the magnitude (number) calculated using the equation

$$\mu H = \sum_{i=1}^{n} \vec{Hi}/N$$

where $\vec{Hi}$ is the vector sum of the hydrophobicity of each residue of helix length, *N*. In addition, the mean hydrophobicity (H) was also calculated using the equation

$$H = \sum_{i=1}^{n} Hi/N$$

where *Hi* is the hydrophobicity of each residue in helix length *N* (60). The values for residue hydrophobicities were established by Fauchere et al. (61). Heliquest (http://heliquest.ipmc.cnrs.fr/) was used to screen specific protein determinants, or the complete proteome of *M. smegmatis*, for potential LD-targeting helices. This online search algorithm slides an 18-residue window of peptides through a user-submitted database, generating helical wheel diagrams of these residues and calculating various helix parameters, including charge (*z*), mean hydrophobicity, and mean hydrophobic moment. Heliquest searches of the *M. bovis* BCD LD-associated proteins were conducted using the following parameters: hydrophobicity, μH ranging from 0.40 to 0.75; mean hydrophobic moment, H ranging from 0.40 to 0.60; *z*, −4 to +4; polar residues, ≥2; uncharged residues (Ser, Thr, Asn, Gln, His), ≥1; no glycine; charged residues, ≤10; no proline at i, i + 3/n − 3, n; no cysteine; no geometric rules; no BlackList. A higher stringency Heliquest search was used to identify $PspA_{Mtb}$-like amphipathic helices present in the *M. smegmatis* proteome (UniProt). These parameters were based on values from $PspA_{Mtb}$, $PspA_{Rho}$, and $PspA_{Eco}$, and included μH ranging from 0.0.467 to 0.546, H ranging from 0.507 to 0.607, *z* from −4 to +4; polar residues of ≥7, uncharged residues (Ser, Thr, Asn, Gln, and His) of ≥2, no glycine, charged residues of ≤5, no proline at i of i + 3/n − 3, n, no cysteine, no geometric rules, and no BlackList.

Mass spectrometry of the LD proteome. The protein concentration of LDs was determined using the QuBit protein assay and instrument (Thermo Fisher Scientific, Waltham, MA). One hundred micrograms of LDs was precipitated by chloroform-methanol extraction and suspended in 50 mM ammonium bicarbonate. The samples were reduced with 10 mM dithiothreitol (DTT) for 30 min at 37°C and alkylated with 50 mM iodoacetamide. Excess alkylating agent was removed by the addition of 10 mM DTT. The samples were digested with mass spectrometry-grade Trypsin Gold (Promega, Madison, WI) at an enzyme-to-substrate ratio of 1:50 overnight at 37°C. Digestion reactions were stopped by the addition of trifluoroacetic acid to a final concentration of 0.1%. The samples were then desalted and processed by Zip-Tip C_{18} columns (MilliporeSigma, Burlington, MA). For each sample, approximately 5 μg of tryptic peptides were loaded via an autosampler (AS-2; Eksigent Technologies Inc.) onto a 100-μm inside diameter (i.d.) trapping column that was hand packed with 2.5 cm of 5-μm 200-Å C_{18} (Magic C_{18} AQ) over 6 min in 2% acetonitrile with 0.1% formic acid. Peptides were eluted from the trapping column onto a 75-μm i.d. analytical column that was hand-packed with 10 cm of 3-μm 200-Å C_{18} (Magic C18 AQ). Elution occurred over 180 min on a 2 to 98% buffer B gradient at a flow rate of 300 nl/min delivered by a NanoLC 2D high-pressure liquid chromatography (HPLC) pump (AB Sciex Eskigent). Buffer A was 0.1% formic acid in H_2O and buffer B was 0.1% formic acid in acetonitrile. The HPLC effluent was directly coupled to the nanoelectrospray ionization source of an LTQ-Orbitrap Velos hybrid mass spectrometer (Thermo Fisher Scientific). Precursor ion scans were collected with one internal lock mass at a resolution setting with a resolution of 60,000 for full MS followed by data-dependent and targeted MS/MS acquisitions of the 10 most abundant ions. The normalized collision energy was set to 35. Dynamic exclusion, monoisotopic precursor selection, and predicted ion injection time were enabled. This was done in technical triplicates for each of three independent biological experiments. The LC-MS/MS data were analyzed with MaxQuant software (version 1.2.2.5) (62) using a UniProtKB *Mycobacterium smegmatis* reference proteome database through MaxQuant's built-in Andromeda search engine. Default parameters were set and protein identification and quantification were performed using the MaxLFQ label-free quantification algorithm previously described. Default parameters in MaxQuant were used wherever applicable. Briefly, variable modifications included protein N-terminal acetylation and oxidized methionine. Carbamidomethylated cysteine was the only fixed modification specified. Full trypsin specificity was selected as digestion mode, and maximum missed cleavages were set to 2. Peptides with lengths of a minimum of 7 amino acids were considered, with both the peptide and protein false discovery rate (FDR) set to 1%. Precursor mass tolerance was set to 20 ppm for the first search and 4.5 ppm for the main search. Product ions were searched with a mass tolerance of 20 ppm. Protein identification required a minimum of three peptides with at least one razor or unique peptide. Label-free quantification was performed using quantities of unique and razor peptides and required a minimum of three peptides. Identified proteins that could be reconstructed from a set of peptides are "grouped" and termed protein groups. The top matched or leading candidate in a protein group is defined as the protein with the greatest number of identified peptides within the group. Protein groups marked as contaminant, reverse, or "identified by site only" in MaxQuant results were discarded.

Statistical analysis of $PspA_{Mtb}$ localization. The abundance of $PspA_{Mtb}$ or H1-GFP chimeras was quantified by densitometry using ImageLab (Bio-Rad, Hercules, CA). The relative abundance of protein in the LD fraction, or in the cytoplasm plus membrane fraction, was expressed as a percentage of the total protein signal detected in all three fractions, which was set at 100%. The values shown represent the average percentages of proteins present determined from three independent cultures prepared and processed in parallel. Statistical significance was determined by a two-tailed, unpaired *t* test with assumed unequal variance.

SUPPLEMENTAL MATERIAL

Supplemental material for this article may be found at https://doi.org/10.1128/JB.00240-18.

SUPPLEMENTAL FILE 1, PDF file, 1.4 MB.

SUPPLEMENTAL FILE 2, XLSX file, 0.1 MB.

ACKNOWLEDGMENTS

This work was supported by a grant from the Potts Foundation to T.C.Z.

We thank Dara Frank, Jenifer Coburn, and Blake Hill for helpful discussions regarding the study.

REFERENCES

1. Anonymous. 2017. WHO world tuberculosis report 2017. World Health Organization, Geneva, Switzerland. http://www.who.int/tb/publications/global_report/gtbr2017_main_text.pdf.
2. Garton NJ, Christensen H, Minnikin DE, Adegbola RA, Barer MR. 2002. Intracellular lipophilic inclusions of mycobacteria *in vitro* and in sputum. Microbiology 148:2951–2958. https://doi.org/10.1099/00221287-148-10-2951.
3. Caire-Brändli I, Papadopoulos A, Malaga W, Marais D, Canaan S, Thilo L, de Chastellier C. 2014. Reversible lipid accumulation and associated division arrest of *Mycobacterium avium* in lipoprotein-induced foamy macrophages may resemble key events during latency and reactivation of tuberculosis. Infect Immun 82:476–490. https://doi.org/10.1128/IAI.01196-13.
4. Daniel J, Kapoor N, Sirakova T, Sinha R, Kolattukudy P. 2016. The perilipin-like PPE15 protein in *Mycobacterium tuberculosis* is required for triacylglycerol accumulation under dormancy-inducing conditions. Mol Microbiol 101:784–794. https://doi.org/10.1111/mmi.13422.

5. Daniel J, Maamar H, Deb C, Sirakova TD, Kolattukudy PE. 2011. *Mycobacterium tuberculosis* uses host triacylglycerol to accumulate lipid droplets and acquires a dormancy-like phenotype in lipid-loaded macrophages. PLoS Pathog 7:e1002093. https://doi.org/10.1371/journal.ppat.1002093.
6. Deb C, Lee C-M, Dubey VS, Daniel J, Abomoelak B, Sirakova TD, Pawar S, Rogers L, Kolattukudy PE. 2009. A novel in vitro multiple-stress dormancy model for *Mycobacterium tuberculosis* generates a lipid-loaded, drug-tolerant, dormant pathogen. PLoS One 4:e6077. https://doi.org/10.1371/journal.pone.0006077.
7. Elamin AA, Stehr M, Spallek R, Rohde M, Singh M. 2011. The *Mycobacterium tuberculosis* Ag85A is a novel diacylglycerol acyltransferase involved in lipid body formation. Mol Microbiol 81:1577–1592. https://doi.org/10.1111/j.1365-2958.2011.07792.x.
8. Baek SH, Li AH, Sassetti CM. 2011. Metabolic regulation of mycobacterial growth and antibiotic sensitivity. PLoS Biol 9:e1001065. https://doi.org/10.1371/journal.pbio.1001065.
9. Daniel J, Deb C, Dubey VS, Sirakova TD, Abomoelak B, Morbidoni HR, Kolattukudy PE. 2004. Induction of a novel class of diacylglycerol acyltransferases and triacylglycerol accumulation in *Mycobacterium tuberculosis* as it goes into a dormancy-like state in culture. J Bacteriol 186:5017–5030. https://doi.org/10.1128/JB.186.15.5017-5030.2004.
10. Kapoor N, Pawar S, Sirakova TD, Deb C, Warren WL, Kolattukudy PE. 2013. Human granuloma *in vitro* model, for TB dormancy and resuscitation. PLoS One 8:e53657. https://doi.org/10.1371/journal.pone.0053657.
11. Low KL, Rao PSS, Shui G, Bendt AK, Pethe K, Dick T, Wenk MR. 2009. Triacylglycerol utilization is required for regrowth of *in vitro* hypoxic nonreplicating *Mycobacterium bovis* bacillus Calmette-Guerin. J Bacteriol 191:5037–5043. https://doi.org/10.1128/JB.00530-09.
12. Murphy DJ. 2012. The dynamic roles of intracellular lipid droplets: from archaea to mammals. Protoplasma 249:541–585. https://doi.org/10.1007/s00709-011-0329-7.
13. Thiam AR, Farese RV, Jr, Walther TC. 2013. The biophysics and cell biology of lipid droplets. Nat Rev Mol Cell Biol 14:775–786. https://doi.org/10.1038/nrm3699.
14. Walther TC, Farese RV, Jr. 2012. Lipid droplets and cellular lipid metabolism. Annu Rev Biochem 81:687–714. https://doi.org/10.1146/annurev-biochem-061009-102430.
15. Ding Y, Zhang S, Yang L, Na H, Zhang P, Zhang H, Wang Y, Chen Y, Yu J, Huo C, Xu S, Garaiova M, Cong Y, Liu P. 2013. Isolating lipid droplets from multiple species. Nat Protoc 8:43–51. https://doi.org/10.1038/nprot.2012.142.
16. Ding Y, Yang L, Zhang S, Wang Y, Du Y, Pu J, Peng G, Chen Y, Zhang H, Yu J, Hang H, Wu P, Yang F, Yang H, Steinbüchel A, Liu P. 2012. Identification of the major functional proteins of prokaryotic lipid droplets. J Lipid Res 53:399–411. https://doi.org/10.1194/jlr.M021899.
17. Armstrong RM, Adams KL, Zilisch JE, Bretl DJ, Sato H, Anderson DM, Zahrt TC. 2016. Rv2744c is a PspA ortholog that regulates lipid droplet homeostasis and nonreplicating persistence in *Mycobacterium tuberculosis*. J Bacteriol 198:1645–1661. https://doi.org/10.1128/JB.01001-15.
18. Low KL, Shui G, Natter K, Yeo WK, Kohlwein SD, Dick T, Rao SPS, Wenk MR. 2010. Lipid droplet-associated proteins are involved in the biosynthesis and hydrolysis of triacylglycerol in *Mycobacterium bovis* bacillus Calmette-Guerin. J Biol Chem 285:21662–21670. https://doi.org/10.1074/jbc.M110.135731.
19. Manganelli R, Gennaro ML. 2017. Protecting from envelope stress: variations on the phage-shock-protein theme. Trends Microbiol 25:205–216. https://doi.org/10.1016/j.tim.2016.10.001.
20. Joly N, Engl C, Jovanovic G, Huvet M, Toni T, Sheng X, Stumpf MPH, Buck M. 2010. Managing membrane stress: the phage shock protein (Psp) response, from molecular mechanisms to physiology. FEMS Microbiol Rev 34:797–827. https://doi.org/10.1111/j.1574-6976.2010.00240.x.
21. Darwin AJ. 2005. The phage-shock-protein response. Mol Microbiol 57:621–628. https://doi.org/10.1111/j.1365-2958.2005.04694.x.
22. Zhang L, Sakamoto W. 2015. Possible function of VIPP1 in maintaining chloroplast membranes. Biochim Biophys Acta 1847:831–837. https://doi.org/10.1016/j.bbabio.2015.02.013.
23. McDonald C, Jovanovic G, Ces O, Buck M. 2015. Membrane stored curvature elastic stress modulates recruitment of maintenance proteins PspA and Vipp1. mBio 6:e01188-15. https://doi.org/10.1128/mBio.01188-15.
24. McDonald C, Jovanovic G, Wallace BA, Ces O, Buck M. 2017. Structure and function of PspA and Vipp1 N-terminal peptides: insights into the membrane stress sensing and mitigation. Biochim Biophys Acta 1859:28–39. https://doi.org/10.1016/j.bbamem.2016.10.018.
25. Westphal S, Heins L, Soll J, Vothknecht UC. 2001. Vipp1 deletion mutant of synechocystis: a connection between bacterial phage shock and thylakoid biogenesis? Proc Natl Acad Sci U S A 98:4243–4248. https://doi.org/10.1073/pnas.061501198.
26. Gao F, Wang W, Zhang W, Liu C. 2015. α-Helical domains affecting the oligomerization of Vipp1 and its interaction with Hsp70/DnaK in *Chlamydomonas*. Biochemistry 54:4877–4889. https://doi.org/10.1021/acs.biochem.5b00050.
27. Joly N, Burrows PC, Engl C, Jovanovic G, Buck M. 2009. A lower-order oligomer form of phage shock protein A (PspA) stably associates with the hexameric AAA(+) transcription activator protein PspF for negative regulation. J Mol Biol 394:764–775. https://doi.org/10.1016/j.jmb.2009.09.055.
28. Standar K, Mehner D, Osadnik H, Berthelmann F, Hause G, Lünsdorf H, Brüser T. 2008. PspA can form large scaffolds in *Escherichia coli*. FEBS Lett 582:3585–3589. https://doi.org/10.1016/j.febslet.2008.09.002.
29. Kobayashi R, Suzuki T, Yoshida M. 2007. *Escherichia coli* phage-shock protein A (PspA) binds to membrane phospholipids and repairs proton leakage of the damaged membranes. Mol Microbiol 66:100–109. https://doi.org/10.1111/j.1365-2958.2007.05893.x.
30. Hankamer BD, Elderkin SL, Buck M, Nield J. 2004. Organization of the AAA(+) adaptor protein PspA is an oligomeric ring. J Biol Chem 279:8862–8866. https://doi.org/10.1074/jbc.M307889200.
31. Jovanovic G, Mehta P, McDonald C, Davidson AC, Uzdavinys P, Ying L, Buck M. 2014. The N-terminal amphipathic helices determine regulatory and effector functions of phage shock protein A (PspA) in *Escherichia coli*. J Mol Biol 426:1498–1511. https://doi.org/10.1016/j.jmb.2013.12.016.
32. Bouvet S, Golinelli-Cohen MP, Contremoulins V, Jackson CL. 2013. Targeting of the Arf-GEF GBF1 to lipid droplets and Golgi membranes. J Cell Sci 126:4794–4805. https://doi.org/10.1242/jcs.134254.
33. Drin G, Antonny B. 2010. Amphipathic helices and membrane curvature. FEBS Lett 584:1840–1847. https://doi.org/10.1016/j.febslet.2009.10.022.
34. Krahmer N, Guo Y, Wilfling F, Hilger M, Lingrell S, Heger K, Newman HW, Schmidt-Supprian M, Vance DE, Mann M, Farese RV, Jr, Walther TC. 2011. Phosphatidylcholine synthesis for lipid droplet expansion is mediated by localized activation of CTP:phosphocholine cytidylyltransferase. Cell Metab 14:504–515. https://doi.org/10.1016/j.cmet.2011.07.013.
35. Prévost C, Sharp ME, Kory N, Lin Q, Voth GA, Farese RV, Jr, Walther TC. 2018. Mechanism and determinants of amphipathic helix-containing protein targeting to lipid droplets. Dev Cell 44:73.e4–86.e4. https://doi.org/10.1016/j.devcel.2017.12.011.
36. Rowe ER, Mimmack ML, Barbosa AD, Haider A, Isaac I, Ouberai MM, Thiam AR, Patel S, Saudek V, Siniossoglou S, Savage DB. 2016. Conserved amphipathic helices mediate lipid droplet targeting of perilipins 1-3. J Biol Chem 291:6664–6678. https://doi.org/10.1074/jbc.M115.691048.
37. Gautier R, Douguet D, Antonny B, Drin G. 2008. HELIQUEST: a web server to screen sequences with specific alpha-helical properties. Bioinformatics 24:2101–2102. https://doi.org/10.1093/bioinformatics/btn392.
38. Dworkin J, Jovanovic G. 2000. The PspA protein of *Escherichia coli* is a negative regulator of sigma(54)-dependent transcription. J Bacteriol 182:311–319.
39. Elderkin S, Bordes P, Jones S, Rappas M, Buck M. 2005. Molecular determinants for PspA-mediated repression of the AAA transcriptional activator PspF. J Bacteriol 187:3238–3248. https://doi.org/10.1128/JB.187.9.3238-3248.2005.
40. Lanfranconi MP, Alvarez HM. 2016. Functional divergence of HBHA from *Mycobacterium tuberculosis* and its evolutionary relationship with TadA from *Rhodococcus opacus*. Biochimie 127:241–248. https://doi.org/10.1016/j.biochi.2016.06.002.
41. de Lima CS, Marques MA, Debrie AS, Almeida EC, Silva CA, Brennan PJ, Sarno EN, Menozzi FD, Pessolani MC. 2009. Heparin-binding hemagglutinin (HBHA) of *Mycobacterium leprae* is expressed during infection and enhances bacterial adherence to epithelial cells. FEMS Microbiol Lett 292:162–169. https://doi.org/10.1111/j.1574-6968.2009.01488.x.
42. Esposito C, Marasco D, Delogu G, Pedone E, Berisio R. 2011. Heparin-binding hemagglutinin HBHA from *Mycobacterium tuberculosis* affects actin polymerisation. Biochem Biophys Res Commun 410:339–344. https://doi.org/10.1016/j.bbrc.2011.05.159.
43. Lebrun P, Raze D, Fritzinger B, Wieruszeski JM, Biet F, Dose A, Carpentier M, Schwarzer D, Allain F, Lippens G, Locht C. 2012. Differential contribution of the repeats to heparin binding of HBHA, a major adhesin of

Mycobacterium tuberculosis. PLoS One 7:e32421. https://doi.org/10.1371/journal.pone.0032421.
44. Menozzi FD, Bischoff R, Fort E, Brennan MJ, Locht C. 1998. Molecular characterization of the mycobacterial heparin-binding hemagglutinin, a mycobacterial adhesin. Proc Natl Acad Sci U S A 95:12625–12630.
45. Mueller-Ortiz SL, Wanger AR, Norris SJ. 2001. Mycobacterial protein HbhA binds human complement component C3. Infect Immun 69:7501–7511. https://doi.org/10.1128/IAI.69.12.7501-7511.2001.
46. Pethe K, Aumercier M, Fort E, Gatot C, Locht C, Menozzi FD. 2000. Characterization of the heparin-binding site of the mycobacterial heparin-binding hemagglutinin adhesin. J Biol Chem 275:14273–14280. https://doi.org/10.1074/jbc.275.19.14273.
47. Zhang C, Yang L, Ding Y, Wang Y, Lan L, Ma Q, Chi X, Wei P, Zhao Y, Steinbuchel A, Zhang H, Liu P. 2017. Bacterial lipid droplets bind to DNA via an intermediary protein that enhances survival under stress. Nat Commun 8:15979. https://doi.org/10.1038/ncomms15979.
48. Otters S, Braun P, Hubner J, Wanner G, Vothknecht UC, Chigri F. 2013. The first alpha-helical domain of the vesicle-inducing protein in plastids 1 promotes oligomerization and lipid binding. Planta 237:529–540. https://doi.org/10.1007/s00425-012-1772-1.
49. Bigay J, Antonny B. 2012. Curvature, lipid packing, and electrostatics of membrane organelles: defining cellular territories in determining specificity. Dev Cell 23:886–895. https://doi.org/10.1016/j.devcel.2012.10.009.
50. Bansal-Mutalik R, Nikaido H. 2014. Mycobacterial outer membrane is a lipid bilayer and the inner membrane is unusually rich in diacyl phosphatidylinositol dimannosides. Proc Natl Acad Sci U S A 111:4958–4963. https://doi.org/10.1073/pnas.1403078111.
51. Chiaradia L, Lefebvre C, Parra J, Marcoux J, Burlet-Schiltz O, Etienne G, Tropis M, Daffe M. 2017. Dissecting the mycobacterial cell envelope and defining the composition of the native mycomembrane. Sci Rep 7:12807. https://doi.org/10.1038/s41598-017-12718-4.
52. Crellin PK, Luo C-Y, Morita YS. 2013. Chapter 6. Metabolism of plasma membrane lipids in mycobacteria and corynebacteria. *In* Baez RV (ed), Lipid metabolism. InTech, Rijeka, Croatia. https://doi.org/10.5772/52781.
53. Gao Q, Shang Y, Huang W, Wang C. 2013. Glycerol-3-phosphate acyltransferase contributes to triacylglycerol biosynthesis, lipid droplet formation, and host invasion in *Metarhizium robertsii*. Appl Environ Microbiol 79:7646–7653. https://doi.org/10.1128/AEM.02905-13.
54. Hayashi JM, Luo CY, Mayfield JA, Hsu T, Fukuda T, Walfield AL, Giffen SR, Leszyk JD, Baer CE, Bennion OT, Madduri A, Shaffer SA, Aldridge BB, Sassetti CM, Sandler SJ, Kinoshita T, Moody DB, Morita YS. 2016. Spatially distinct and metabolically active membrane domain in mycobacteria. Proc Natl Acad Sci U S A 113:5400–5405. https://doi.org/10.1073/pnas.1525165113.
55. Law JD, Daniel J. 2017. The mycobacterial Rv1551 glycerol-3-phosphate acyltransferase enhances phospholipid biosynthesis in cell lysates of *Escherichia coli*. Microb Pathog 113:269–275. https://doi.org/10.1016/j.micpath.2017.10.050.
56. Pol A, Gross SP, Parton RG. 2014. Review: biogenesis of the multifunctional lipid droplet: lipids, proteins, and sites. J Cell Biol 204:635–646. https://doi.org/10.1083/jcb.201311051.
57. Allen B. 1998. Mycobacteria, p 15–30. *In* Parish T, Stoker N (ed), Mycobacteria protocols, vol 101. Humana Press, New York, NY.
58. White MJ, Savaryn JP, Bretl DJ, He H, Penoske RM, Terhune SS, Zahrt TC. 2011. The HtrA-Like serine protease PepD interacts with and modulates the *Mycobacterium tuberculosis* 35-kDa antigen outer envelope protein. PLoS One 6:e18175. https://doi.org/10.1371/journal.pone.0018175.
59. Guo XV, Monteleone M, Klotzsche M, Kamionka A, Hillen W, Braunstein M, Ehrt S, Schnappinger D. 2007. Silencing essential protein secretion in *Mycobacterium smegmatis* by using tetracycline repressors. J Bacteriol 189:4614–4623. https://doi.org/10.1128/JB.00216-07.
60. Eisenberg D, Weiss RM, Terwilliger TC. 1982. The helical hydrophobic moment: a measure of the amphiphilicity of a helix. Nature 299:371–374. https://doi.org/10.1038/299371a0.
61. Fauchere J, Pliska V. 1983. Hydrophobic parameters pi of amino-acid side chains from the partitioning of N-acetyl-amino-acid amides. Eur J Med Chem 18:369–975.
62. Cox J, Mann M. 2008. MaxQuant enables high peptide identification rates, individualized p.p.b.-range mass accuracies and proteome-wide protein quantification. Nat Biotechnol 26:1367. https://doi.org/10.1038/nbt.1511.
63. Ding Y, Yang L, Zhang S, Wang Y, Du Y, Pu J, Peng G, Chen Y, Zhang H, Yu J, Hang H, Wu P, Yang F, Yang H, Steinbüchel A, Liu P. 2012. Identification of the major functional proteins of prokaryotic lipid droplets. J Lipid Res 53:399–411. https://doi.org/10.1194/jlr.M021899.
64. Chen Y, Ding Y, Yang L, Yu J, Liu G, Wang X, Zhang S, Yu D, Song L, Zhang H, Zhang C, Huo L, Huo C, Wang Y, Du Y, Zhang H, Zhang P, Na H, Xu S, Zhu Y, Xie Z, He T, Zhang Y, Wang G, Fan Z, Yang F, Liu H, Wang X, Zhang X, Zhang MQ, Li Y, Steinbüchel A, Fujimoto T, Cichello S, Yu J, Liu P. 2014. Integrated omics study delineates the dynamics of lipid droplets in Rhodococcus opacus PD630. Nucleic Acids Res 42:1052–1064. https://doi.org/10.1093/nar/gkt932.